Warming^UP GOO

Geothermie & Opslag Opschaling

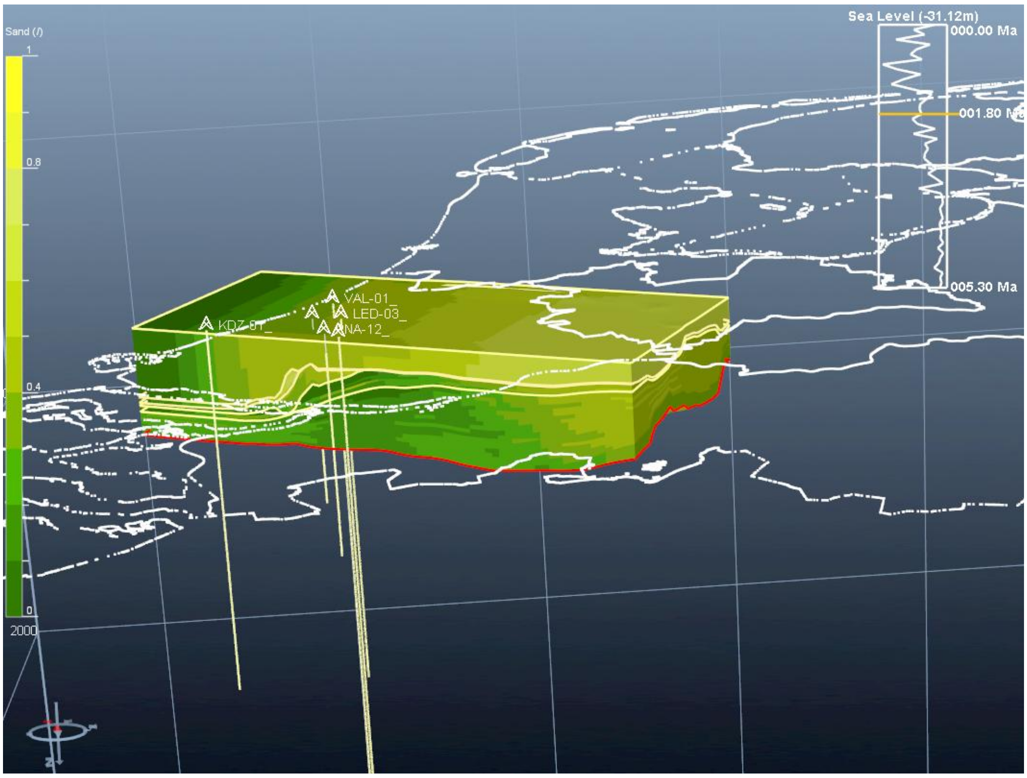


# Stratigraphic Forward Modelling of the Maassluis and Oosterhout Formations

**by**

Marianne van Unen, Sander Houben, Eva De Boever, Elisabeth Peters

4 augustus 2026

Stratigraphic Forward Modelling of the Maassluis and Oosterhout Formations

Marianne van Unen, Sander Houben, Eva De Boever, Elisabeth Peters

Reviewer: Chris van Baak (Deltares)

The work for this report was carried out as part of the WarmingUP Geothermal and Storage Scaling project (WarmingUP *GOO*). This was made possible by a subsidy from the Netherlands Enterprise Agency (RVO) under the Mission-driven Research, Development and Innovation (MOOI) subsidy scheme, known at RVO under project number MOOI322012. WarmingUP *GOO* contributes to MOOI mission B *Built Environment* and contributes to the innovation theme *Sustainable collective heat supply*.

Projectnummer
060.52558

Keywords
Stratigraphic Forward modelling, Oosterhout Formation, Maassluis Formation

Jaar van publicatie
2026

Meer informatie
Marianne van Unen
T 06 29154352
E Marianne.vanunen@tno.nl

## Table of contents

# Summary

Aquifer Thermal Energy Storage (ATES) can be an important element in the sustainable-energy mix. Former studies have indicated that sedimentary deposits situated at depths of about 200 to 500 meters could have good potential for HT-ATES (high temperature aquifer thermal energy storage). Such depths often correspond to the Oosterhout and Maassluis Formations in the Netherlands, which were deposited during the Pliocene to Early Pleistocene. This depth domain has relatively poor data density and is relatively poorly characterized because in the past the focus was on deep conventional hydrocarbon and geothermal reservoirs or shallow groundwater intervals.

To improve our understanding of these formations and support characterization we are using DionisosFlow Stratigraphic Forward Modelling (SFM) software. SFM software simulates the transport and deposition of sediments through time and space. For the study area, which covers most of the province of South-Holland, lithostratigraphic borehole interpretations, a provisional seismic interpretation of key horizons and paleobathymetry estimates are used as model input to simulate the deposition during the Plio-Pleistocene.

The results of the SFM are subsequently used to improve the geostatistical modelling of the distribution of lithology in a smaller, more detailed model. Sequential Indicator Simulation and Multiple-Point Statistics are used as geostatistical methods. In the latter method, patterns can be reproduced based on a training image. In this study, the SFM results are used as the training image.

The SFM model area consists of two zones. In a small part of the west of the model area, provisional seismic interpretations provide internal clinoform structural geometries within the Oosterhout and Maassluis Formations. Precise biostratigraphic age constraints for these clinoform units were not available. The larger size of the study area is needed, in order to arrive at a functional SFM, in which sediment flow and accumulation can be balanced. Two sediment supply sources were considered in the SFM: a larger one from the south-east and a smaller one from the south-west, representing major river input. In the SFM, the lithology of seven deep wells, also considered by Veldkamp et al. (2026) were used for manual calibration. For the subsequent geostatistical modelling, a much larger number of wells (79) was used to constrain lithology.

The results of the SFM match fairly well to the observed lithology in the wells. The fine grained, muddy layers reflect the clinoform base whereas the sand-dominated layers reflect the upper part of the clinoforms. The SFM however only reproduced an evident clinoform structure, in the area where the seismically-interpreted clinoform surfaces were used as a bathymetric model input.

Possible improvements could be made by adding further seismic interpretations, making use of biostratigraphic age-dating of the respective structures, and by including more wells in a larger area. The subsequent geostatistical modelling at the regional scale (20 x 30 km) gave more detail in the sand thickness maps including a qualitative estimate of the uncertainty. In the south of the model area, much more clay occurs in both formations. In the north-west, the Maassluis Formation is more clayey and the top of the Oosterhout Formation is sandy compared to the rest of the model.

# Samenvatting

Warmteopslag in aquifers kan een belangrijk bijdrage leveren aan een duurzame energie mix. Eerdere studies hebben laten zien dat sedimentaire afzettingen op dieptes van ongeveer 200 tot 500 meter goede potentie voor hoge temperatuur opslag kunnen hebben. Op deze dieptes komen vaak de Oosterhout en Maassluis Formaties voor, welke tijdens het Plioceen tot Vroeg Pleistoceen zijn afgezet. De data dichtheid en ondergrondse karakterisatie op deze diepte is relatief laag, doordat in het verleden vooral de focus was op diepe conventionele olie, gas en geothermische reservoirs of ondiepe grondwater intervallen.

Om een beter begrip van deze formaties te krijgen en als toevoeging op de karakterisatie ervan, gebruiken wij de DionisosFlow Stratigrafisch Voorwaards Modellering (SFM) software. Voor het studiegebied, welke het merendeel van de provincie Zuid-Holland beslaat, zijn lithostratigrafische interpretaties van boringen, een verkennende seismische interpretatie van belangrijke laagvlakken en paleobathymetrische schattingen gebruikt als modelinvoer om de depositie gedurende het Plio-Pleistoceen te simuleren.

De resultaten van de SFM worden daarna gebruikt voor het verbeteren van geostatistische modelleringen van de verbreiding van de lithologie in een kleiner, gedetailleerder model. Sequential Indicator Simulation en Multiple-Point Statistics zijn de gebruikte geostatische methodes. In de laatste methode, worden patronen in de lithologie gereproduceerd gebaseerd op een trainingsbeeld. In deze studie worden de SFM resultaten gebruikt als trainingsbeeld.

Het SFM modelgebied bestaat in essentie uit twee delen. In een klein gebied in het westen van het modelgebied, laten voorlopige seismische interpretaties interne clinoform structuren zien in de Oosterhout en Maassluis Formaties. Exacte biostratigrafische leeftijden van deze clinoforms waren niet beschikbaar. Het grotere gedeelte van het studiegebied is nodig om een functioneel SFM te krijgen, waar sediment aanvoer en accumulatie kunnen worden gebalanceerd. Twee aanvoerrichtingen van het sediment zijn gebruikt in het SFM: een grotere bron vanuit het zuidoosten, en een kleinere bron vanuit het zuidwesten, welke belangrijke rivieraanvoer representeren. In het SFM, is de lithologie van zeven diepe boringen, welke ook waren meegenomen door Veldkamp et al., (2026), gebruikt voor handmatige kalibratie. Voor de geostatistische modellering die daarna is uitgevoerd, is een veel grotere hoeveelheid boringen (79) meegenomen om de lithologie te bepalen.

De resultaten van het SFM komen goed overeen met de beschreven lithologie in de boringen. De fijnkorrelige, kleiige onderste laag representeert de onderste laag van de clinoforms en meer zandig gedomineerde lagen zijn representatief voor het bovenste deel van de clinoforms. Het SFM reproduceerde echter alleen duidelijke clinoform structuren in het gebied waar de seismische geïnterpreteerde clinoforms waren gebruikt als een bathymetrie input in het model. Verbeteringen zijn mogelijk door het maken van meer seismische interpretaties, gebruikmakend van biostratigrafische leeftijd datering van de desbetreffende structuren, en door het betrekken van meer boringen in een groter gebied. De geostatistische modellering op regionale schaal (20 x 30 km) gaf meer detail in de zanddiktekaart inclusief een kwalitatieve schatting van de onzekerheid. Deze zanddiktekaart toont dat in het noordwesten de Maassluis Formatie meer kleiig is dan in de rest van het gebied, terwijl de top van de Oosterhout Formatie juist meer zandig is vergeleken met de rest van het gebied.

# 1 Introduction

To reach the greenhouse gas emission reduction targets, a transition to a sustainable energy solution must be made. Due to the intermittency of many renewable energy resources and fluctuations in energy demand, stability and flexibility of the energy system needs to be improved. This can be done by Aquifer Thermal Energy Storage, with an increasing interest for High Temperature – Aquifer Thermal Energy Storage (HT-ATES) in the shallow subsurface of the Netherlands. In HT-ATES systems, high temperature (>60°C) excess heating is stored temporarily in aquifers in the subsurface. Preferably, this is done at shallow depths between 200-1500 m as drilling costs will be too high for deeper aquifers. Usually, storage is done in a setting where an aquifer or sandstone reservoir is overlain and underlain by a sealing structure (e.g. clay layers), so that the heat loss will be minimized.

In the past, the focus of exploration and production was on deep conventional reservoirs or shallow groundwater intervals. Low well coverage and limited seismic data of at the depth interval between 200-1500 m in many parts of the Netherlands hamper the Tertiary-Quaternary sedimentary characterization. In the Warming^UP *GOO* project, several activities are performed that are aimed at improving the characterization of this intermediate depth domain at both regional and national scale and estimate HT-ATES and low temperature geothermal potential. Activities that are part of this project are for example national scale seismic interpretation and mapping of the Breda Subgroup and Oosterhout Formation (Altenburg and van Unen, 2025) and estimating the HT-ATES potential in the region of The Hague (Veldkamp et al., 2026).

In this report, a workflow is developed in which Stratigraphic Forward Modelling (SFM) of sedimentary systems is used to improve the characterization of the Maassluis and Oosterhout formations. The Pliocene – Pleistocene Oosterhout and Maassluis formations represent potential targets for ATES developments (Pluymaekers et al., 2013). The workflow consists of two parts:

- Stratigraphic forward simulation at the regional scale of the province of South-Holland.
- An investigation of how the results from the SFM model can be used to guide geostatistical modelling of the lithofacies at smaller scales.

The geometries and characteristics of clastic sedimentary systems are principally driven by a combination of the by rate and type of sediment supply and the available accommodation space in the sedimentary basin. Energy input and transport parameters are also imporant. Changes in accommodation space depend on tectonics and sea level fluctuations (Kuhlmann, 2004; Hawie et al., 2015). The economic benefits of clastic sedimentary shelf systems are well known due to their high potential reservoirs with hydrocarbon accumulations (Kombrink et al., 2012). Stratigraphic Forward Modelling (SFM) tools can improve our understanding of clastic sedimentary by generating 4D simulations of the stratigraphic thickness, reservoir properties and distributions away from well- and seismic control (Ducros et al., 2023). The benefit of this tool is that it is based on actual physics in sedimentary processes, thereby providing geologically consistent subsurface models (Hawie et al., 2015). When based on detailed geological conceptual constraints, this enables geologically correct mapping of the targeted sedimentary intervals and allows to improve knowledge on the sedimentary architecture of the modeled interval.

By using DionisosFlow (by BeicipFranlab), a Stratigraphic Forward Modelling (SFM) tool, a geological model of the facies distribution of the Oosterhout and Maassluis formations in the province of South-Holland has been made (Figure 1.1). Within this study we aim to improve the interpolation quality of the sand-clay bodies for the Pliocene - Pleistocene intervals between selected well locations.

Constraints on the input data for the SFM are of prime importance for simulating the sedimentary evolution and building maps in a reliable manner. Critical input is data and information on the depth maps and time constraints, but also the sediment transport system, and the tectonic and sedimentary evolution. To derive this input, information has been gathered from literature, newly interpreted horizons (depth markers) and facies descriptions of selected well data (Veldkamp et al., 2026) has been used. Newly interpreted internal geometries (clinoforms) from seismic interpretation studies (Veldkamp et al., 2026) are used as intermediate horizons (Figure 1.1). Manual calibration of the modelling results was performed on interpreted well data from Veldkamp et al. (2026).

The manual calibration of the lithofacies distribution predicted by the SFM is cumbersome and only a limited number of wells is included. This means that the lithofacies distribution from SFM is not consistent with all the available data. Therefore, we investigated in what way the SFM results can be used in more local models including additional well data to improve the lithofacies distribution modelling compared to traditional lithofacies modelling which is only based on well data (e.g. in REGIS).

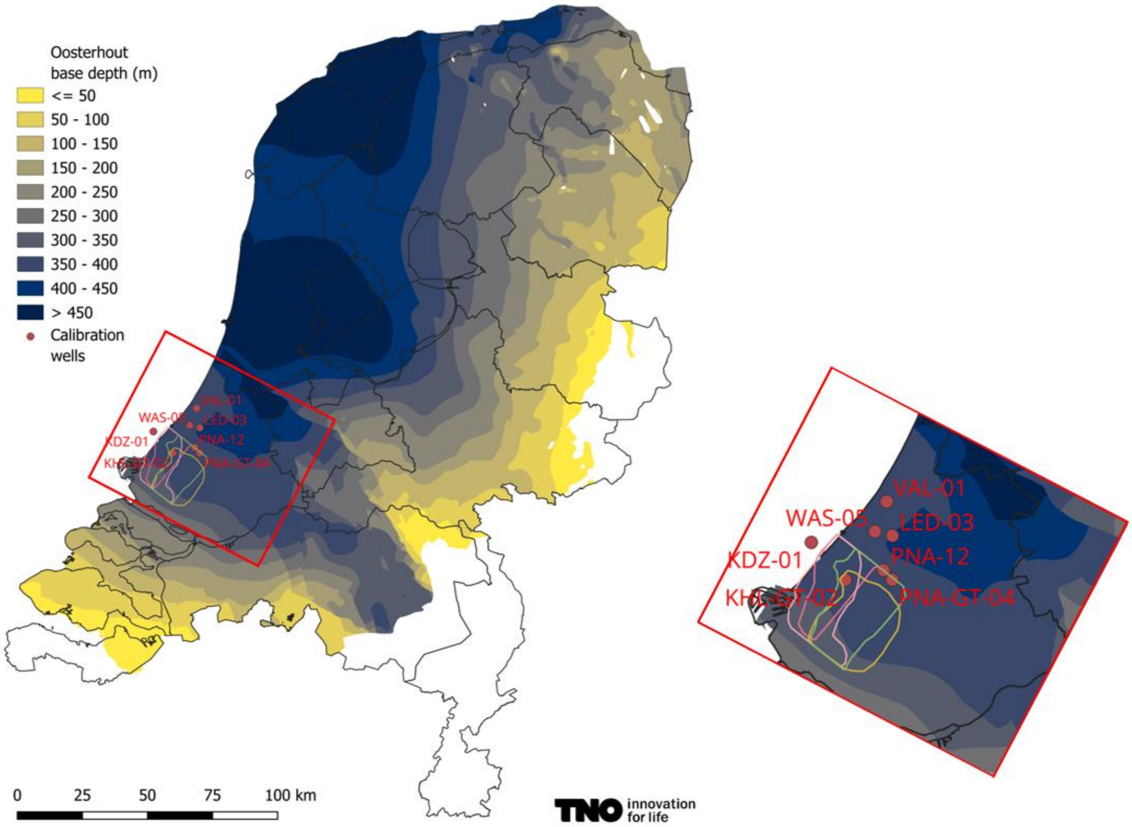


Figure 1.1 Oosterhout base depth map from DGM (Digital Geological Model) (TNO - GDN, 2021). Red square is the location of the simulation area in DionisosFlow. Red dots are the key wells used for the SFM from Veldkamp et al (2026). Outlines orange: clinoform 1, green: clinoform 2, red: clinoform 3 and pink: clinoform 4 (see also lower right inset for an enlargement of the study area and interpreted clinoforms).

# 2 Geological context

By Pliocene to early Pleistocene times (~5.3 - 2 million years ago) the area now comprising the province of South Holland, was situated in shallow marine to coastal environments. The main, open-marine North Sea Basin, was located to the north-northwest (Figure 2.1).

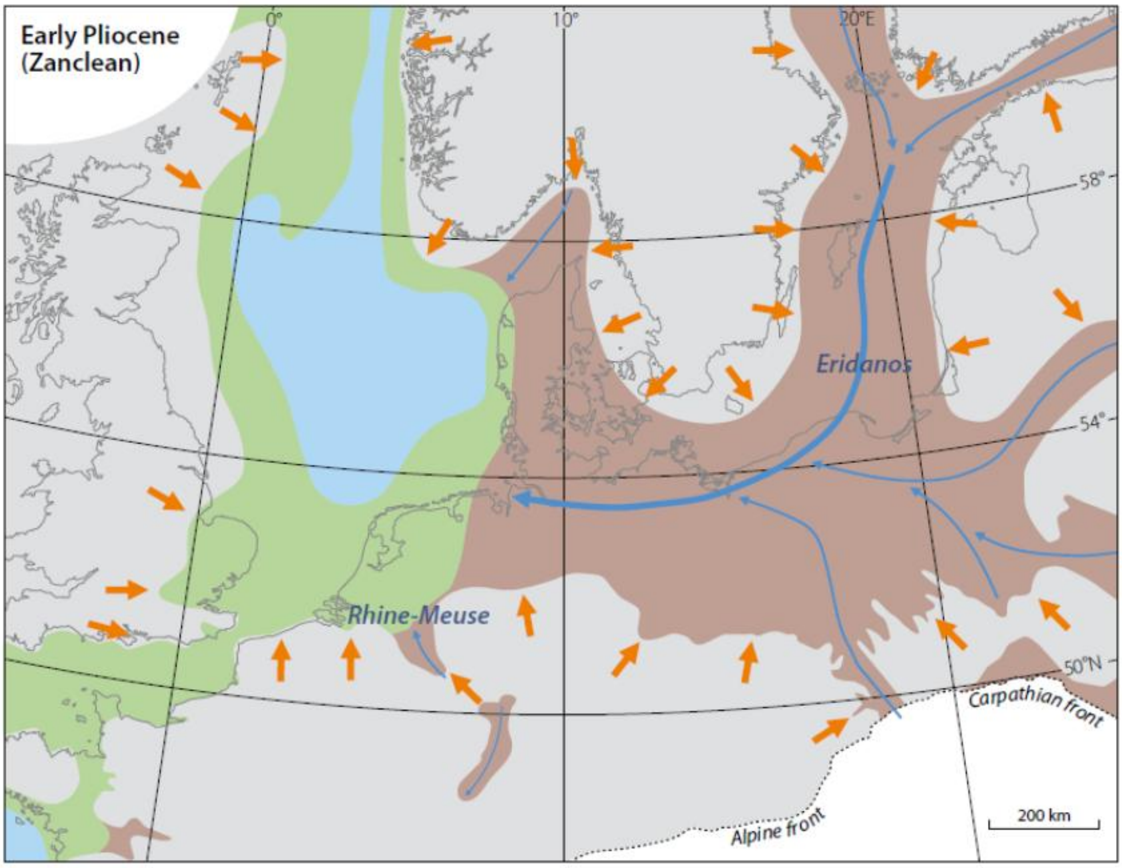


Figure 2.1 Paleogeographic map showing of NW-Europe during early Pliocene times, adapted from Gibbard and Lewin (2016) and Munsterman et al. (2025)

The primary sediment source was thought to be from the southeast (the Rhine-Meuse system), initially confined to an active graben system (Roer Valley Graben, RVG). Smaller river systems may have provided sediment input from the elevated area that now comprises western Belgium. The major baltic-derived Eridanos fluvial system was unlikely to have substantially provided sediment to the Zuid Holland Area (Overeem et al., 2002; Westerhof et al., 2008; Busschers et al., 2025; Figure 2.2). The above implies that the large majority of sediment input for the SFM comes from a southeasterly direction, with a theoretical contribution from the Belgian rivers as well and that the clinoforms develop in a NW-dipping direction (see also Veldkamp et al., 2026).

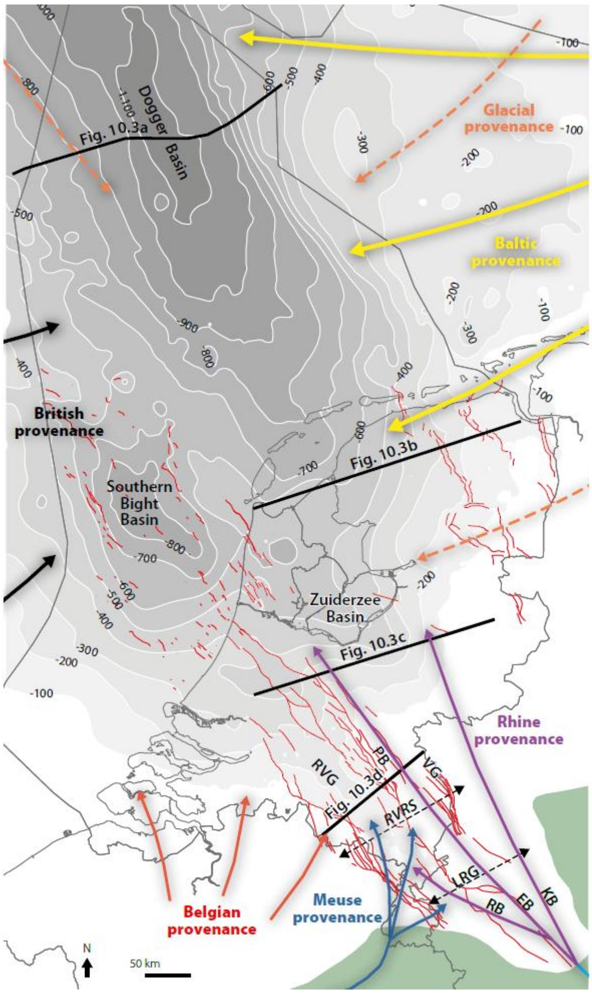


Figure 2.2 Depth map of the base of the Quaternary (Pleistocene, isolines: depth below modern MSL) with main tectonic elements, faults (in red) sediment-transport pathways. Depths above -100 m MSL not indicated. LRG = Lower Rhine Graben, RB = Roer Block, EB = Erft Block, KB = Köln Block, RVRS = Roer Valley Rift System, RVG = Roer Valley Graben, PB = Peel Block, VG = Venlo Graben. Adapted from Busschers et al. (2025).

By early-mid Pliocene times (~5.3 – 3.5 million years ago), relative sea-level was high, as major northern hemisphere ice-sheet build-up had not yet started to develop. An overall fine-grained, locally condensed sequence of Oosterhout Formation sediments accumulated across much of Zuid Holland. Coarser grained, fluvial to deltaic sediments were confined to the southeastern part of the RVG (Limburg) and the eastern border with Germany. By late Pliocene times (3.2 Ma), an initial phase of glacioeustatic fall (M2-glaciation, Lisiecki and Raymo, 2005; Dearing Crampton-Flood et al., 2020) led the initiation of progradation and clinoform development across much of the southern North Sea shelf. This generation of clinoform development is not yet systematically seismically mapped by TNO-GSN. However, these clinoforms are likely to be represented by the oldest generation of clinoforms mapped by Veldkamp et al. (2026,).

The base of the Pleistocene/Quaternary (2.58 Ma) marks next major step in ice-sheet expansion and consequent sea-level fall, with the near-permanent establishment of NH ice-sheets (Lisiecki and Raymo, 2005). This is observed as a renewed progradational sequence across much of the North Sea shelf. Note that this sequence is of earliest Pleistocene (Gelasian age), albeit these strata may still be assigned to the Oosterhout Fm., on lithostratigraphic grounds.

A striking intensification of glacial-interglacial amplitudes variation is now considered to have caused a major sequence stratigraphic boundary, at a level ***within*** the early Pleistocene (Gelasian, 2.4 Ma, Marine Isotope Stage 95, see Noorbergen et al., 2015 and Busschers et al., 2025). This led to the development of sand-dominated delta-and coastal plain settings across much of Zuid Holland. This marks the base of the Maassluis Formation on seismic profiles, the Maassluis Formation is typically characterized by parallel or very low angle progradational reflectors. Note however, that basin-ward in the North Sea, more high angle shelf clinoforms, similar to the Oosterhout clinoforms develop.

The above implies that the clinoforms that were interpreted by Veldkamp et al. (2026, Figure 2.2) in the Rotterdam area correspond to two generations of Oosterhout progradation (viz., a late Pliocene (OO-1) one and an earliest Pleistocene one (Gelasian, OO-2), deposited between 2.6 and 2.4 Ma). This hypothesized relationship between the locally interpreted clinoform geometries and their timing requires further biostratigraphic validation. Nevertheless, it lasted a substantial period, until the mid-Pleistocene (1.8 million years ago) until truly fluvial conditions (Peize-Waalre formations) were established over Zuid Holland.

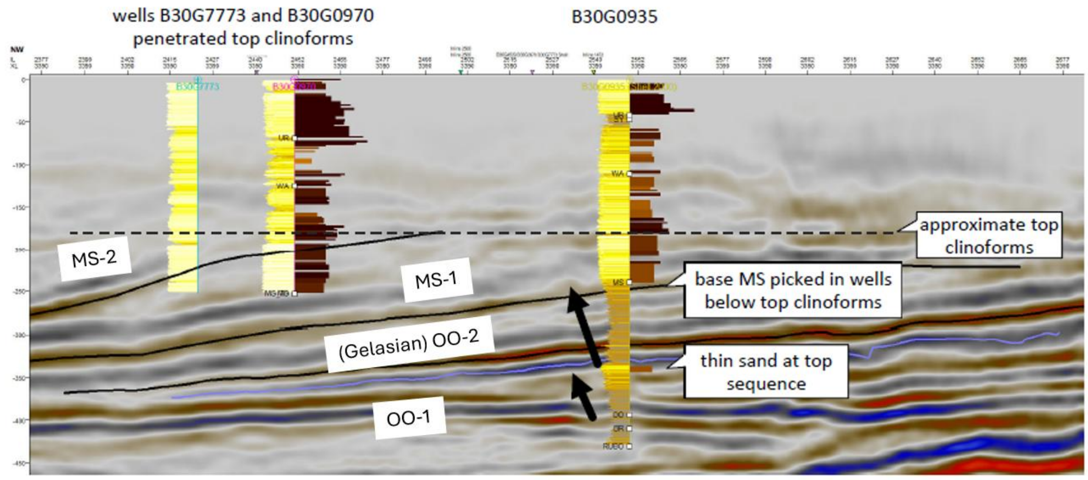


Figure 2.3 NW-SE Seismic depth section taken from the L3NAM1990C (Monster) cube. Borehole trajectories are projected on the seismic line. Lithostratigraphic picks, gamma-ray log profile (left) and sand median grain size (right) are indicated. Lithostratigraphic picks are indicated on the borehole trajectories (SY=Stramproy, UR=Urk, WA=Waalre, MS=Maassluis, OO=Oosterhout, BR=Breda, RUBO=Rupel Boom, base markers). The respective clinoforms generations are marked (OO-1, OO-2, MS-1, MS-2). Modified after Veldkamp et al. (2026).

For the time being, we here rely on existing lithostratigraphic interpretations to place well data in stratigraphic context. Veldkamp et al. (2026) interpreted four clinoform generations (Figure 2.3). These have been used for the SFM in this study (Figure 1.1). From well log interpretations, low net-to-gross values are observed in the Oosterhout Formation with a low sand content of less than 19% (Table 2.1 based on Veldkamp et al., 2026). Well log interpretations of the Maassluis Formation show a distinctly higher sand content (high net-to-gross (NtG)) of 40 to 90% with thin silt layers (Table 2.1).

Table 2.1 Deep wells with petrophysical analysis from (Veldkamp et al., 2026), showing gross thickness, NtG (net-to-gross in %) and porosity (por in %). The formation boundaries are based on the well tops as available on nlog.nl, which can deviate from the DGM depth. For KHL-GT-02 and PNA-GT-04 insufficient information was available to determine porosity.

| # | well name | Maassluis Formation | | | Oosterhout Formation | | |
|---|---|---|---|---|---|---|---|
| | | Thickness (m) | NtG (%) | Por (%) | Thickness (m) | NtG (%) | Por (%) |
| 1 | KDZ-01 | 132 | 24 | 25 | 143 | 8 | 5 |
| 2 | KHL-GT-02 | 194 | 44 | - | 92 | 3 | - |
| 3 | LED-03 | 151 | 53 | 25 | 144 | 1 | 5 |
| 4 | PNA-12 | 85 | 88 | 35 | 176 | 3 | 10 |
| 5 | PNA-GT-04 | 200 | 47 | - | 70 | 0 | - |
| 6 | VAL-01 | 105 | 67 | 15 | 164 | 8 | 10 |
| 7 | WAS-05 | 127 | 45 | 20 | 113 | 19 | 10 |

# 3 Methodology and data

4D Stratigraphic Forward Modelling is simulates the distribution of sand, silt and clay. To simulate the sedimentary evolution in a reliable and representative manner, constraints on the input data for the SFM is of prime importance. Data and information have been gathered from a literature study, and interpreted well data and seismic data (Veldkamp et al., 2026) that cover the Pliocene – Pleistocene sequences in the The Hague region. Critical input data and knowledge necessary for SFM are the: depth maps and age constraints, sediment transport system (e.g. course, direction, water discharge, amount of sediments shed by source areas) and the sedimentary (depositional) evolution (e.g. amount of subsidence, accommodation space, sedimentation rate, uplift, erosion) with time in the studied and surrounding intervals.

The SFM model created by DionisosFlow covers approximately the province of South Holland. This model occupies an area of about 65 x 75 km, has a cell size of 1 km, and a vertical resolution of 5000 years (Figure 1.1).

## *3.1* Depth horizons

As bottom surface, the base Oosterhout Formation from the Digital Geological Model (DGM) was used (TNO - GDN, 2021). The base Pliocene age (5.3 Ma) was taken for this horizon. As the top, the top of the Maassluis Formation from DGM was used, assuming a top Gelasian age of 1.8 Ma (Figure 3.1). Intermediate horizons were derived from the seismic interpretation study (Veldkamp et al., 2026), in which the top depths of clinoform structures for the Pliocene/Pleistocene intervals were interpreted. Four of these clinoforms have been used within our DionisosFlow model (Figure 2.3 and Figure 3.1). Because the interpreted clinoforms do not cover the entire model area, the intermediate horizons have been extrapolated using the DionisosFlow software. This extrapolation is not ideal and could be improved by either following a general structural trend outside the interpretation area, or by doing additional seismic interpretations in these extrapolated areas. However, this was beyond the scope of the current project. The enhanced size of the model compared to the area with the clinoforms (Figure 1.1) was necessary to avoid boundary effects. The results of the SFM should only be interpreted in the area in which the wells and clinoforms are located.

For the SFM, an age has to be assigned to the intermediate horizons. Ages of 3.55 Ma (clinoform surface 1, top OO-1), 2.68 Ma (clinoform surface 2, Top OO-2), 2.24 Ma (clinoform surface 3, Top MS-1) and 2.02 Ma (clinoform surface 4, Top MS-2) have been used for these horizons. However, these age estimates are very uncertain due to a scarcity of data, and therefore these may need to be revised in the future.

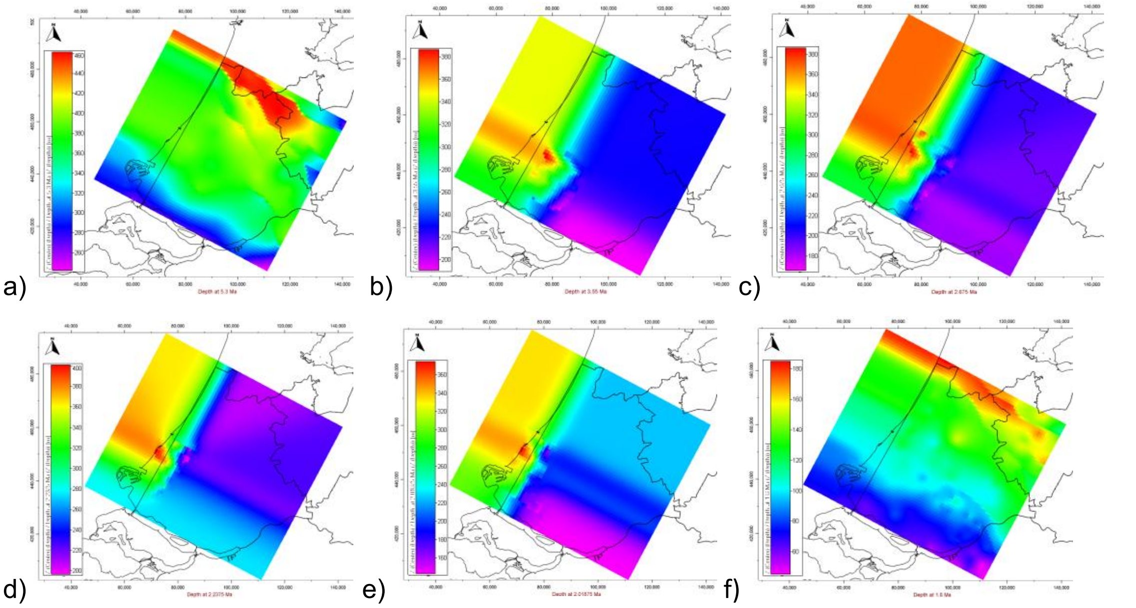


Figure 3.1 Input depth maps of the a) base Oosterhout Formation (5.3Ma), b) Clinoform 1 (3.55Ma?), c) Clinoform 2 (2.68Ma?), d) Clinoform 3 (2.24Ma?), e) Clinoform 4 (2.02Ma?), and f) Top Maassluis Formation (1.8Ma). Ages indicated with ? indicate values with considerable uncertainty related to the resolution in time that can be obtained with biostratigraphy in these sediments. Note that the clinoform maps have been extrapolated outside the interpretation area using the interpolation function in the DionisosFlow software, which is therefore not reliable outside the interpretation area. Note that the colour scale for depth differs between the panels.

## 3.2 Accommodation space

Estimating accommodation space through time is an important step in building a stratigraphic forward model as it is the parameter guiding the volume available to be filled at each time step. In this study, six depth maps based on the horizons presented in the previous paragraph (associated with six different time steps) are used together with a constant paleobathymetry map at each of these time steps in order to calculate subsidence maps through time (Subsidence = delta paleobathymetry + thickness). The thickness maps are being calculated from the base depth maps of the various horizons used in the model. This information together with the sea level curve used (from Rohling et al., 2022) provide the software with the accommodation space through time.

## 3.3 Paleobathymetry estimates

As part of the Warming^UP *GOO* project, national scale seismic interpretation and mapping of the Oosterhout Formation was performed (Altenburg and van Unen, 2025). From this, a national scale paleobathymetry estimate could be derived for the Oosterhout Formation by analyzing internal clinoform heights using the method of Hijma et al. (2025). This method assumes that the top of the unit approximates the sea level at the time of deposition. The paleo water depth is then approximated from the internal clinoform heights and the total thickness. The maximum clinoform height over the total thickness of the unit at that location is calculated and used as a percentage to approximate the paleobathymetry from the thickness maps.

The percentage of the clinoform heights compared to the full Oosterhout thickness was roughly estimated to be around 13.5% based on the clinoform structures from the national scale SCAN seismic lines (see Figure 3.2 and Appendix A for the clinoform estimates). Therefore, we assumed the paleobathymetry to be 13.5% of the Oosterhout base depth map (Figure 3.2). However, because of the small number of clinoforms identified and as the SCAN seismic lines are absent for the region of South-Holland uncertainty remained in the applicability of this value to the South-Holland region.

In a later stage the clinoform heights from the interpreted seismic lines in the South-Holland region could be analyzed (Veldkamp et al., 2026). Here, the percentage of the clinoform heights compared to the full Oosterhout thickness was larger and roughly estimated to be between 23-28% with an average of 26%.

As the clinoform heights that are observed vary and thus also the paleobathymetry, a sensitivity analysis was done to check for the impact of the paleobathymetry on the results. A run was done with a 26% of the Oosterhout Fm depth map. The results did not demonstrate major changes and showed a slight decrease in the amount of silt and increase in sand (ca. 5-10%), and a thickness difference of only a few meters.

As the results of the two model runs did not show large differences, we continued with our first modelling results, but it must be noted that the paleobathymetry in this model is most likely an underestimation based on the clinoform structures in South Holland.

Furthermore, the paleobathymetry was kept constant through time for the following reasons:

- the intermediate horizons are indicated by clinoform structures (with uncertain age), and the base Maassluis Formation was not taken as a horizon into our model (because clinoform 4 extends through both the Oosterhout and Maassluis Formations).
- Additionally, (the top of) the clinoforms in the Maassluis Formation are difficult to determine from seismic data and therefore we assumed that the paleowaterdepth of the Oosterhout Formation is applicable for the Maassluis Formation.

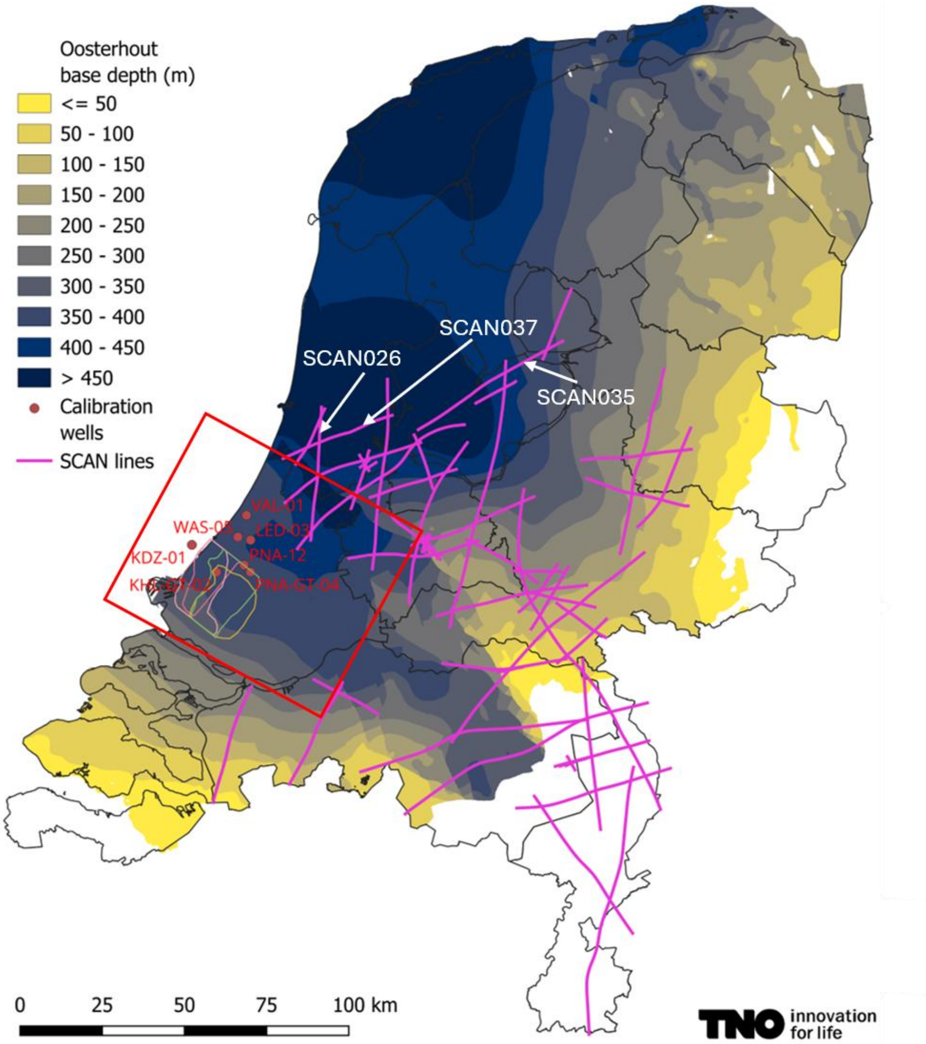


Figure 3.2 SCAN seismic lines (purple lines) for which the paleobathymetry was derived through clinoform structures from lines SCAN026, 035 and 037 (see also Appendix A). For further explanation of the symbols see Figure 1.1.

## 3.4 Sediment supply and fluvial discharge

Sediment entry points have been estimated based on available paleogeographic information (Figure 3.3). Two sediment source positions have been used in the model, one from the SE (S1, the Rhine-Meuse system in Figure 2.2) and one from the SW (S4, representing the Belgian provenance). Initially, the magnitude of sediment supply and water discharge was based on recent analogue comparison and recent Rhine-Meuse river sediment supply and water discharge (Middelkoop et al., 2010; sediment supply of 4500 $km^3$/Ma and water discharge of 4700 $m^3$/s). However, as we focus on a smaller area in the western part of the Netherlands and not a national model of the entire Netherlands, the amount of sediment supply and fluvial discharge was reduced compared to the ones found in (Middelkoop et al., 2010). The sediment supply and fluvial discharge were altered based on our calibration results, to derive a fit to the well data while keeping other parameters stable. The resulting numbers are listed in Figure 3.3.

**S1**

Supply: [km³/Ma] / Fluvial Discharge: [m³/s] / Sediment proportion: [/]

| Age [Ma] | Supply | Fluvial Discharge | Clay | Sand | Silt |
|---|---|---|---|---|---|
| Average | 602.05 | 273.4 | 0.26 | 0.26 | 0.48 |
| 1.8 | 1300 | 500 | 0.3 | 0.25 | 0.45 |
| 2.0187 | 1250 | 500 | 0.14 | 0.4 | 0.46 |
| 2.2375 | 0 | 30 | 0.14 | 0.26 | 0.6 |
| 2.675 | 0 | 30 | 0.14 | 0.26 | 0.6 |
| 3.55 | 180 | 160 | 0.14 | 0.26 | 0.6 |
| 5.3 | 240 | 160 | 0.14 | 0.26 | 0.6 |

**S4**

Supply: [km³/Ma] / Fluvial Discharge: [m³/s] / Sediment proportion: [/]

| Age [Ma] | Supply | Fluvial Discharge | Clay | Sand | Silt |
|---|---|---|---|---|---|
| Average | 478.88 | 155.6 | 0.22 | 0.47 | 0.31 |
| 1.8 | 1150 | 350 | 0.2 | 0.5 | 0.3 |
| 2.0187 | 980 | 350 | 0.2 | 0.5 | 0.3 |
| 2.2375 | 0 | 20 | 0.4 | 0.2 | 0.4 |
| 2.675 | 0 | 20 | 0.4 | 0.2 | 0.4 |
| 3.55 | 50 | 40 | 0.4 | 0.2 | 0.4 |
| 5.3 | 120 | 40 | 0.4 | 0.2 | 0.4 |

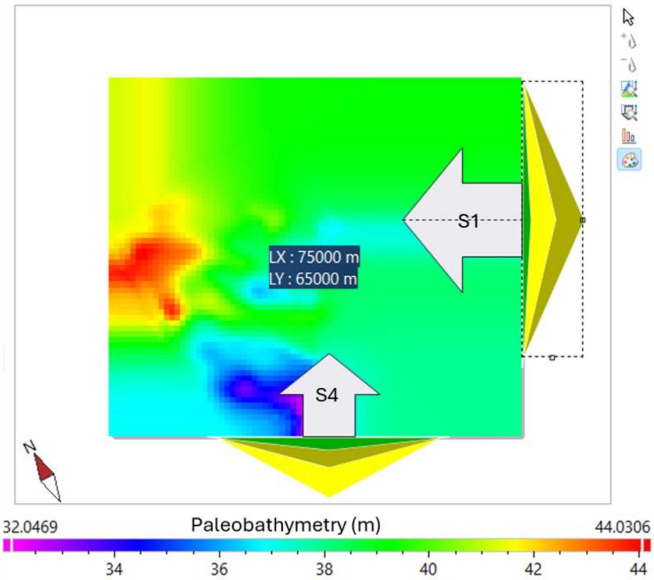


Figure 3.3 Input parameters of the reported model. The paleobathymetry map demonstrates the orientation of incoming sources. S1 from the SE and S4 from the SW (note: that S2 and S3 are not presented in this report as these were part of another larger national model for the Oosterhout Fm). Upper table: sediment input for S1, lower table: sediment input for S4.

## 3.5 Calibration

Several types of data can be used to manually calibrate DionisosFlow models. This includes thickness data, wireline logs and lithofacies logs based on core descriptions. In this case, the model is calibrated by comparing formation thickness as recorded in the calibration wells with the thickness maps calculated from the depth maps in Figure 3.1. Subsequently the model facies are compared to lithology descriptions, referred to as 'lithofacies' here, of 7 selected wells provided by Veldkamp et al. (2026). Those wells are KDZ-01, KHL-GT-02, LED-03, PNA-12, PNA-GT-04, VAL-01, WAS-05, as listed in Table 2.1. The distinct lithofacies that are used relate to grain size categories: sand, silt and clay.

# 4 SFM results and interpretation

## 4.1 Calibration results

Due to the large uncertainty in the extrapolation of the clinoform structures outside the area of interpretation and in age constraints of the clinoform depth maps, only the total modelled thickness was calibrated to the total input thickness between the base Oosterhout and the top Maassluis Formation. Additionally, the lithologies of the model were matched to the 7 selected wells. The total thickness and the lithofacies results from the model show a good fit with the wells data, with a thickness error of <9% (Figure 4.1 and Figure 4.2). The modelling results of the internal clinoform markers do show an overall shallower position compared to the clinoform depth data. However, the overall structural trend of the modelled clinoforms are in agreement with the seismic interpretation. For most wells the modelled lithofacies are in approximate agreement with the those described in calibration wells. However, within well PNA-GT-04 more sand is expected in the lower part of the Oosterhout Formation based on the well logs. The lithology interpretation in this well is further discussed in Chapter 5, section 5.5.

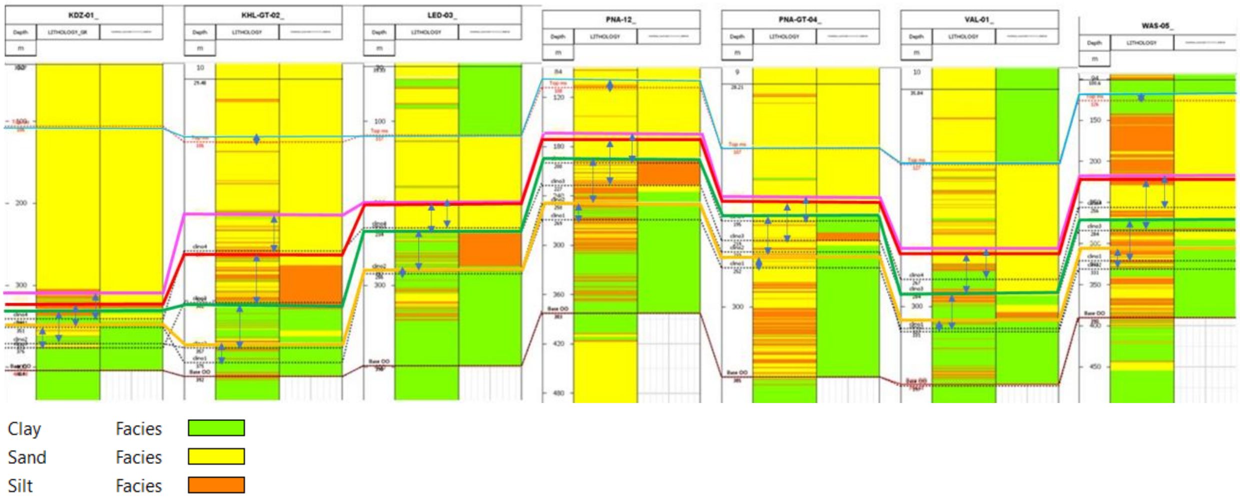


Figure 4.1 Calibration of the modelled markers coloured lines (where orange: clinoform 1, green: clinoform 2, red: clinoform 3, pink: clinoform 4, and blue: top Maassluis) with the well markers (dotted black lines). The arrows represent the offset between the modelled markers and well data markers. Note that the base Oosterhout modeled marker is on the well data marker. The lithofacies calibration is done by comparing the left side of each well which is the input facies and right side of the well is the simulated lithofacies. Lithofacies: yellow= sand, orange= silt and green= clay.

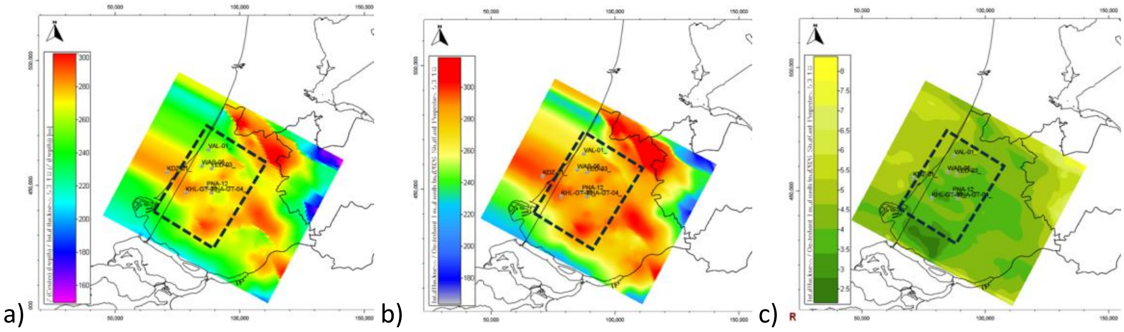

Figure 4.2 Maps demonstrating a good thickness match between the a) total input thickness data, b) modelled total thickness, which can also be indicated by the c) Thickness difference error map in %. The black dashed rectangle indicates the area in which the model is constrained by data.

## 4.2 Clinoform geometries

From the 3D SFM model the clinoform geometries can be seen, which are also interpreted in seismic data (Veldkamp et al., 2026). The modelling results show that the clinoform structures are prograding towards the north-west and show a coarsening upward sequence with more sandy layers in the upper parts and more clayey layers in the lower part (Figure 4.3 where more sand is yellow and clay is green). Such trends can also be observed in interpreted well logs and seismic data. The sea level curve of Rohling et al. (2022) suggests repetitive sea level drops, which could be related to the building out of the clinoforms and their internal coarsening upward trend (Figure 4.3). From the 3D model and cross sections within the SFM model it is also visible that the Oosterhout Formation shows a more clayey content and the Maassluis Formation is more sandy (Figure 4.3b-d).

The modelling results show that first clay and later sand is being deposited, which demonstrates that two separate systems are formed rather than one clinoform system. This result can be explained by the changes in sediment supply from the different sources through time that were used in the model, which is filling the (constant) bathymetry through time (Figure 4.3). Whether this interpretation in the model is a good representation of the real system is not clear with the current information. However, as discussed in Chapter 2, major changes occurred in the conditions during the period that has been simulated, so it is to be expected that there are changes in the sediment supply.

When comparing cross-sections from our model to seismic sections (Figure 4.3d) the overall geometry looks similar.

a) b) c) d)

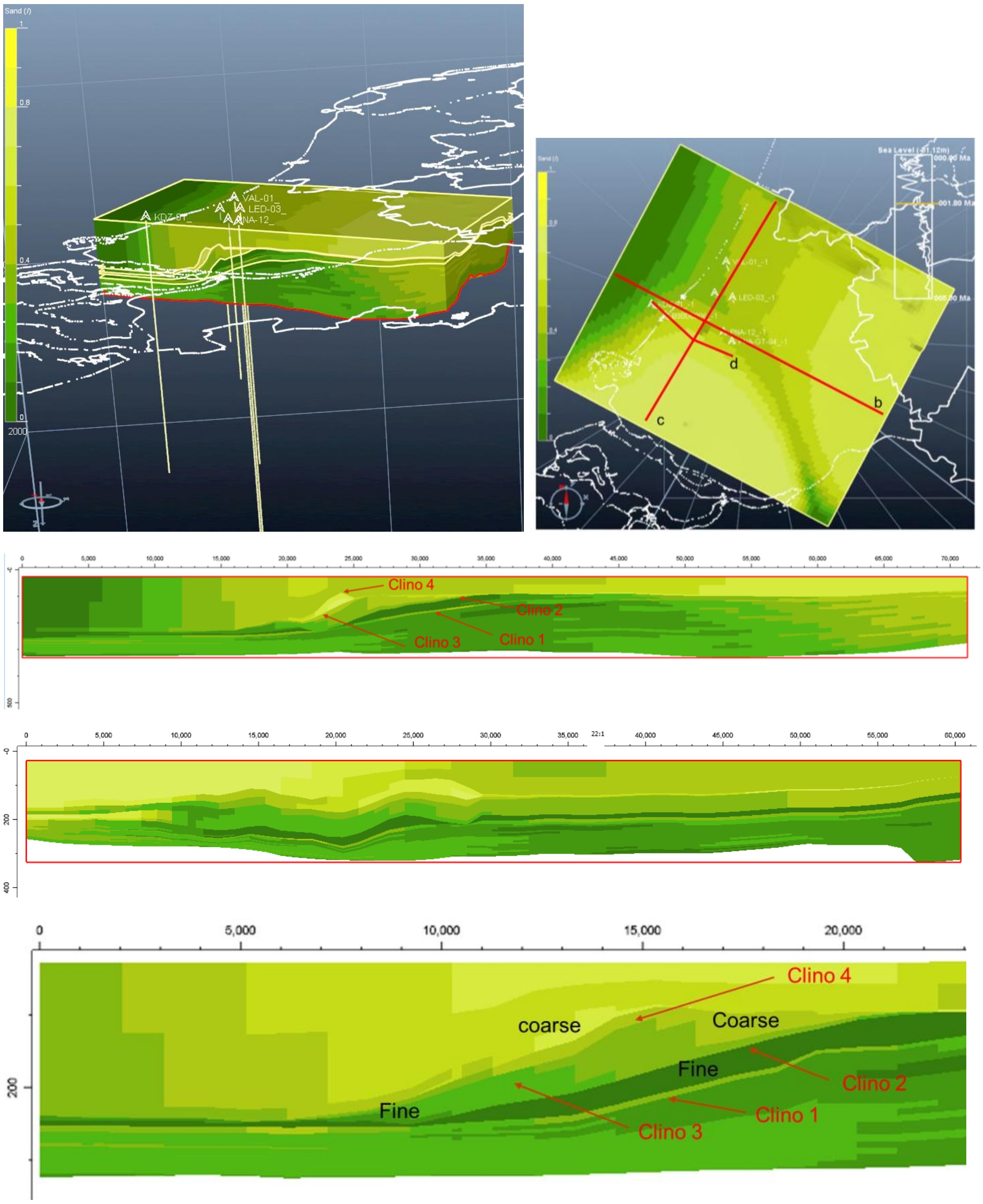


Figure 4.3 SFM model demonstrating the sand (yellow) - clay (green) distribution. a) 3D view. Red lower line = base Oosterhout Fm, Top yellow line = top Maassluis Fm, intermediate yellow lines are the clinoforms 1 (deepest) to 4 (shallowest). On the right a sand content map at 1.8Ma is displayed with the location of the cross sections in b, c and d. In the upper right corner the sea level fluctuations through time is visible. b) large scale NW-SE oriented cross-section along dip of S1. c) large scale N-S oriented cross section along dip of S4. d) Upper Figure: Seismic section at approximately the same location as the cross-section below (NUOO = base Oosterhout depth, NUMS = base Maassluis depth). The cross-section extends from the NW (left) to the SE (right) See brown line in figure on the right for the position of the cross-section and seismic section.

## 4.3 Sand thickness maps and net-to-gross

Maps of the net sand thickness and sand net to gross were created from the 3D SFM for base Oosterhout to top Maassluis formations (Figure 4.4). These maps together can identify good quality reservoirs, by identifying areas with high net sand thickness and high sand net to gross.

The postprocessing output shows highest net sand thicknesses in the southeast with values of up to 290 m of sand thickness. However, this is on the edge of the model area and outside of the model part that is well constrained by data. In the area which is better constrained (indicated by the dashed black rectangle in Figure 4.4), the largest sand thickness occurs in north-westerly direction. This area also has the highest net to gross values.

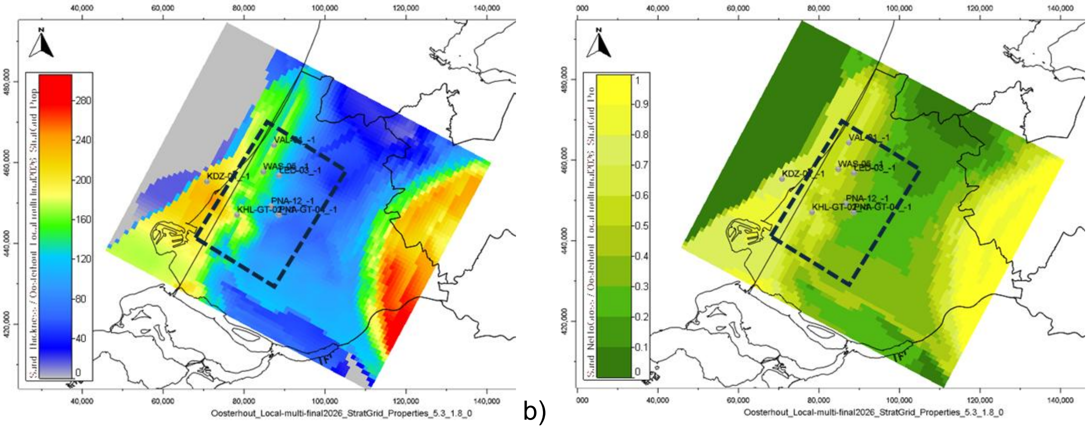


a) b)

Figure 4.4. Maps demonstrating the a) net sand thickness, b) net-to-gross of the base Oosterhout to top Maassluis Formation. The black dashed rectangle indicates the area in which the model is constrained by data.

# 5 Use of SFM results for geostatistical 3D lithology modelling

## 5.1 Introduction

The results of the SFM are at a relatively coarse scale and their calibration is constrained to a limited number of wells (seven). In the area of The Hague more wells with lithological information are available, in particular in the Maassluis Fm, but using these wells for calibration of the SFM results is currently very cumbersome. Using only the well data to model the lithological distribution (which is done in REGIS and many shallow model approaches) is also suboptimal, because in that case the geological information of the presence of clinoforms is ignored. Therefore in this chapter it is investigated how modeled results of the SFM can be combined with more well data to constrain the lithological distribution. To do this, we will apply geostatistical methods for facies modelling, such as sequential indicator simulation and multiple point statistics to the area with most well data in the area modelled with SFM.

## 5.2 Methodology and input data

**Test area**

A grid is created in the area around The Hague in South-Holland which has the largest density of wells with lithological information and falls in the area in which the SFM results are constrained to well data and the clinoform structures. The outline is shown in Figure 5.1. In the same figure, the outline of the SFM results is shown as well as the outline of a detailed model of the Maassluis bottom sand that was mapped by Veldkamp et al. (2026) and which will be used to compare the results to.

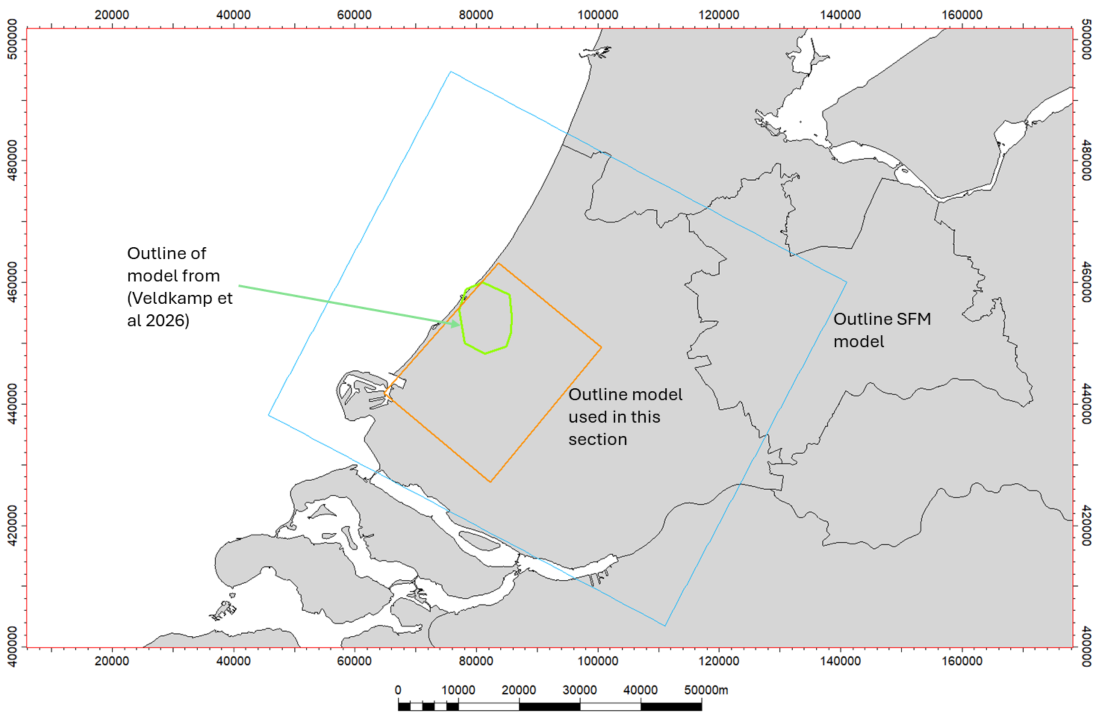


Figure 5.1 Map showing the outlines of the different model areas: the outline of the SFM results (large blue square), smaller model area used here (orange rectangle) and the outline of the small model of the Maassluis Fm bottom sand described in (Veldkamp et al 2026; green polygon), which is used for comparison. Black lines indicate province boundaries

**Grid**

The total size of the model area is around 22 x 29 km, with a rotation of ~40° to the east (Figure 5.1). A grid is created with a horizontal resolution of 200 m. In vertical direction 30 layers are used, resulting in an average cell height of around 9 m. Two grid versions with different layer geometry are created:

- A cartesian grid which is based on DGM v2.2 surfaces (TNO-GDN, 2021): the top of the Maassluis Fm is used as the top of the grid and the bottom Oosterhout Formation ise used as the bottom of the grid. These surfaces were also used for the SFM model. The bottom Maassluis/top Oosterhout is used as an intermediate surface to create separate zones for the Maassluis and Oosterhout formations. Because the DGM Maassluis and Oosterhout surfaces in this area are almost horizontal, the resulting grid is a quite regular cartesian grid with 200 x 200 x ~9 m cells.
- A grid in which surfaces from the SFM output are used to create the layering geometry. Three surfaces are used:
  - as bottom surface, the bottom of the SFM output is used which is the same as the DGM base Oosterhout.
  - an intermediate surface around the transition from the Oosterhout Formation to the Maassluis Formation is used to guide the layering and divide the model in two zones: a mostly sandy upper zone and a mostly shaly lower zone. The surface is very close to one of the seismically interpreted clinoforms. The difference between this surface and the DGM top Oosterhout/bottom Maassluis is shown in Figure 5.2. The reason for using a surface from the SFM, rather than the interpreted clinoform surface is the need for consistency: the results from the SFM will be mapped to this grid, which would not be possible if the positions of the clinoforms are different.

- a surface which is near the top of the Maassluis Formation as the top of the model. This surface is almost the same as the DGM top Maassluis Formation.

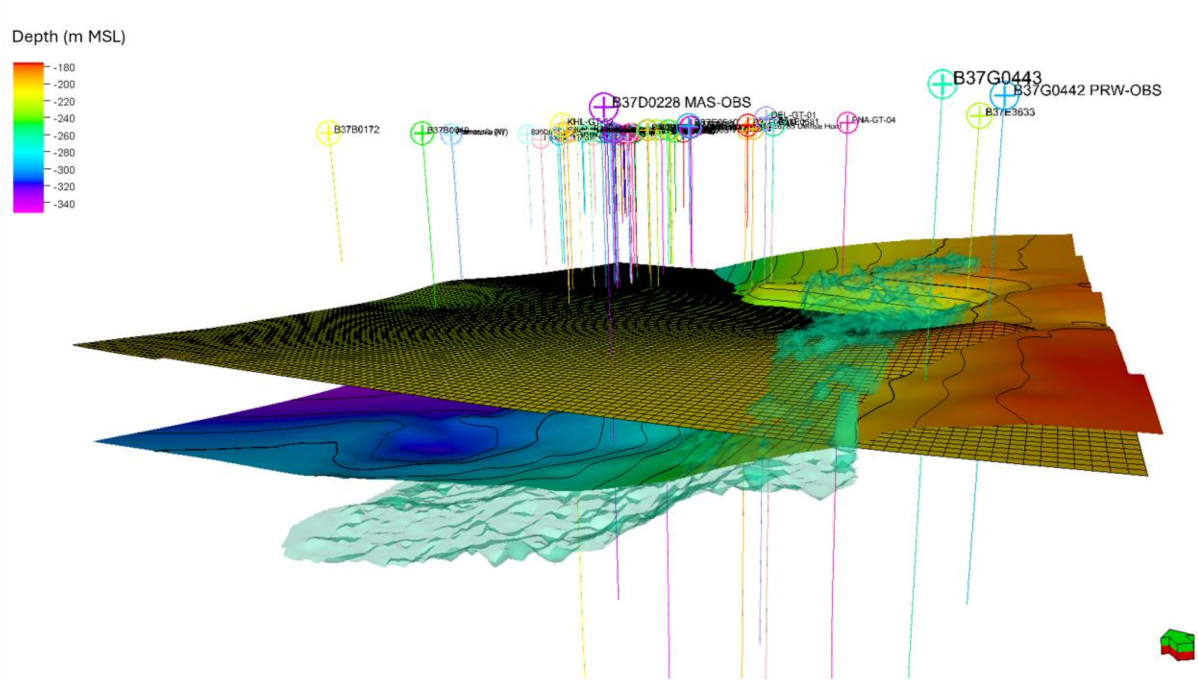


Figure 5.2 Difference between DGM bottom Maassluis Formation/top Oosterhout Formation (the gridded surface) and the surface used in the model based on SFM output (the surface with contours). The partially transparent surface is a clinoform surface interpreted in the seismic data (Veldkamp et al., 2026). View is from the south (green-red arrow indicates north).

**Well data and lithology input**

In total, 79 wells were available in the model area with usable lithology data (see Appendix B for a list of wells). The information from the wells that is used in this case is lithology in terms of sand, silt and clay. Of these 78 wells, only nine wells penetrate the entire model thickness and reach below the Oosterhout Formation. Five of the wells used for the SFM are in the model area and included in this set. For the SFM, only the wells with detailed interpretation from Veldkamp et al. (2026) were used. For the largest part of the wells, the lithology is based on descriptions of the cuttings. For some wells, like those interpreted in Veldkamp et al. (2026), only petrophysical logs are available and no reliable lithological descriptions. For these wells, the lithology is derived from the shale content which is derived from mainly GR (Gamma Ray) or SP (Spontaneous Potential).

The well logs have predominantly sand and clay, with much smaller amounts of silt and very small amounts of shells and 'undefined' (< 0.5%). The lithology 'sand' includes fine, medium and coarse sand in this work. Since shells and peat are not simulated in the SFM, these will not be included in the lithofacies modelling.

In Figure 5.3, a cross section is shown of the cartesian grid. The lithofacies shown on the grid are the lithology results of the SFM mapped to the grid. The cross-section shows the reason for using the second grid: the dipping thinner sand and/or clay layers in a cartesian grid loose continuity which is problematic for flow modelling ("stair-stepping" effect). Also shown are the lithology logs upscaled to the grid at the well locations. Figure 5.4 shows the same picture for the model based on surfaces from the SFM model results. The boundary between the clay-dominated bottom part is now a surface and does not show the "stair-step" effect seen in the cartesian grid.

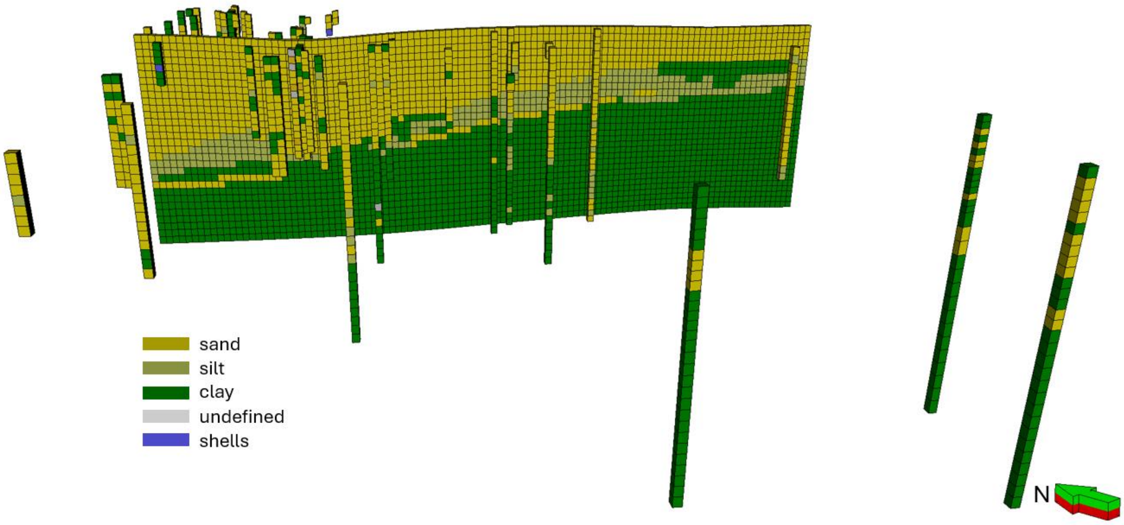


Figure 5.3 Example cross-section (j=45) of the results of the SFM mapped to the cartesian model and upscaled well lithologies in the model area. View from south-west. Green/red arrow indicates north. Vertical exaggeration is 25. Grid blocks are around 200 x 200 x 9 m. Length of the cross section is ~22 km.

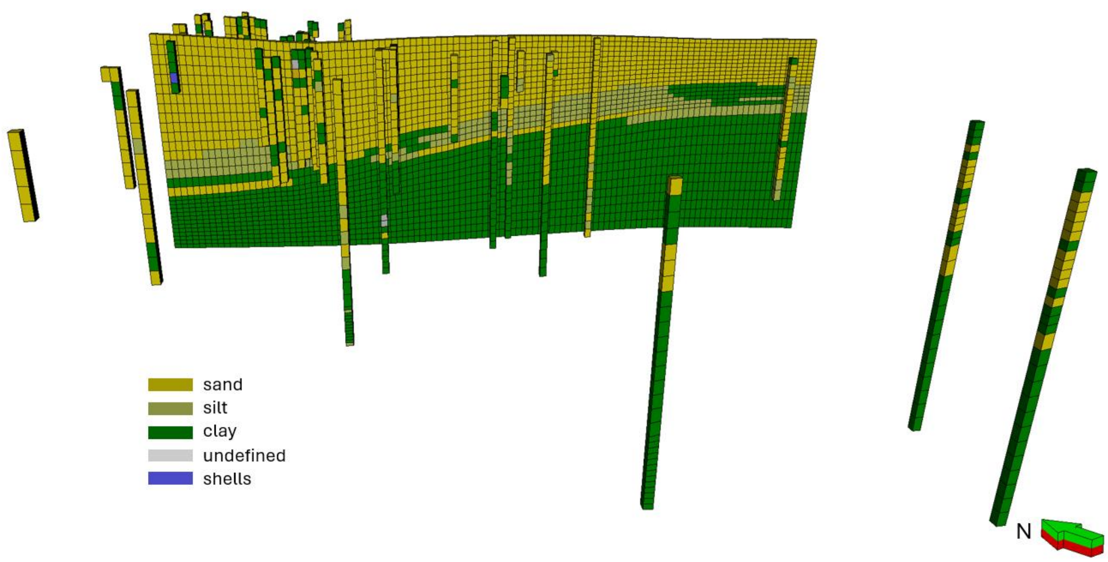


Figure 5.4 Example cross-section (j=45) of the results of the SFM mapped to the grid based on the surfaces from the SFM and upscaled well lithologies in the model area. View from south-east. Green/red arrow indicates north. Vertical exaggeration is 25. Grid blocks are around 200 x 200 x 9 m. length of the cross section is ~22 km.

**Methods**

To create a distributed lithology property, which is constrained to (upscaled) well log data, several methods are available. Two main groups are:

- interpolation methods, such as kriging which result in a single solution. Indicator kriging will be used here because facies are categorical data.
- simulation methods which populate a grid based on algorithms which depend on a random seed. Using a different random seed results in a different facies distribution.

Here the focus will be on the second group of methods, but kriging results will be shown for comparison. The simulation methods used are Multiple Point Statistics (MPS) and Sequential

Indicator Simulation (SIS). Multiple-Point Statistics (MPS) methods can be used to add patterns to simulation of discrete properties (Strebelle, 2002). In MPS, training images are used to represent the spatial relationships between facies which in this case are the lithologies sand, silt and clay. From the training image, statistical relations of the spatial distribution of the facies relative to each other are derived. Training images can be created in different ways, such as object-based modelling. Here the results from the SFM are used to create training images. Sequential Indicator Simulation is a method in which random samples per grid block are taken based on the probability calculated from indicator kriging (Deutsch and Journel, 1998). All methods used in this report are as implemented in Petrel™ 2024.9.

All methods require estimates of the fractions of the different lithologies. These can be derived from the (upscaled) well logs. For this study they can also be derived from the SFM results. The default Petrel workflows generally use the fractions from the upscaled well logs. However, in this case there are two reasons why we don't follow this default. First, there is a severe bias in the distribution of the available wells both in depth and laterally (see the upscaled wells in Figure 5.3). The bias in depth can (partially) be solved by modelling the lithofacies per zone or with a vertical trend, in which the change in the vertical direction can be explicitly applied. The bias in the lateral distribution is more difficult to resolve and that will not be addressed here. Second, we have additional information about the lithofacies distribution from the SFM model. Table 5.1 shows the distribution of the lithofacies for the two models per zone. The results from the SFM show much more clay in the Oosterhout Formation. To be able to honor the well logs, the average from the upscaled well logs and mapped SFM results will be used as input for the lithofacies modelling, which are presented in the last columns of Table 5.1.

Table 5.1 Percentage of the different lithofacies in the two different grids (cartesian and with SFM surfaces) for the upscaled well logs, for the mapped SFM results and to be used in the lithofacies modelling. Please note that the percentages in the upscaled well logs don't add up to 100, because not all lithofacies are included.

| | **Upscaled well logs** | | | | **Mapped SFM results** | | | | **Used in lithofacies modelling** | | | |
|---|---|---|---|---|---|---|---|---|---|---|---|---|
| | Cartesian grid | | SFM surfaces grid | | Cartesian grid | | SFM surfaces grid | | Cartesian grid | | SFM surfaces grid | |
| | MS | OO | Upper | Lower | MS | OO | Upper | Lower | MS | OO | Upper | Lower |
| **Sand** | 77.4 | 18.4 | 74.8 | 17.3 | 79.0 | 11.6 | 77.6 | 0.0 | 78 | 15 | 76 | 9 |
| **Silt** | 3.3 | 13.2 | 3.5 | 14.1 | 6.5 | 5.7 | 8.5 | 2.5 | 5 | 10 | 6 | 9 |
| **Clay** | 18.7 | 67.3 | 21.4 | 66.6 | 14.5 | 82.7 | 14.0 | 97.5 | 17 | 75 | 18 | 82 |

In some methods, also a vertical trend can be used. The vertical trend is created per grid layer and is thus also grid specific. Figure 5.5 shows the vertical trends based on the upscaled wells and the mapped SFM results for the two grids. Figure 5.6 shows the manually created vertical trends to be used in the lithofacies modelling.

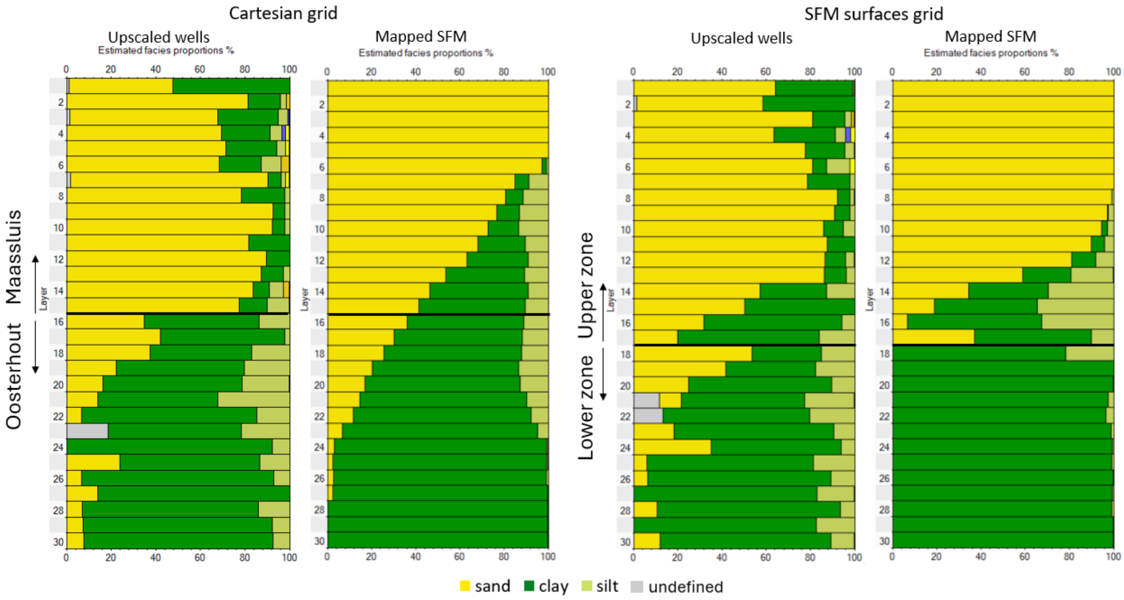


Figure 5.5. Percentage of lithofacies per grid layer for the upscaled cells and mapped SFM results for the model with cartesian grid and for the model based on SFM surfaces.

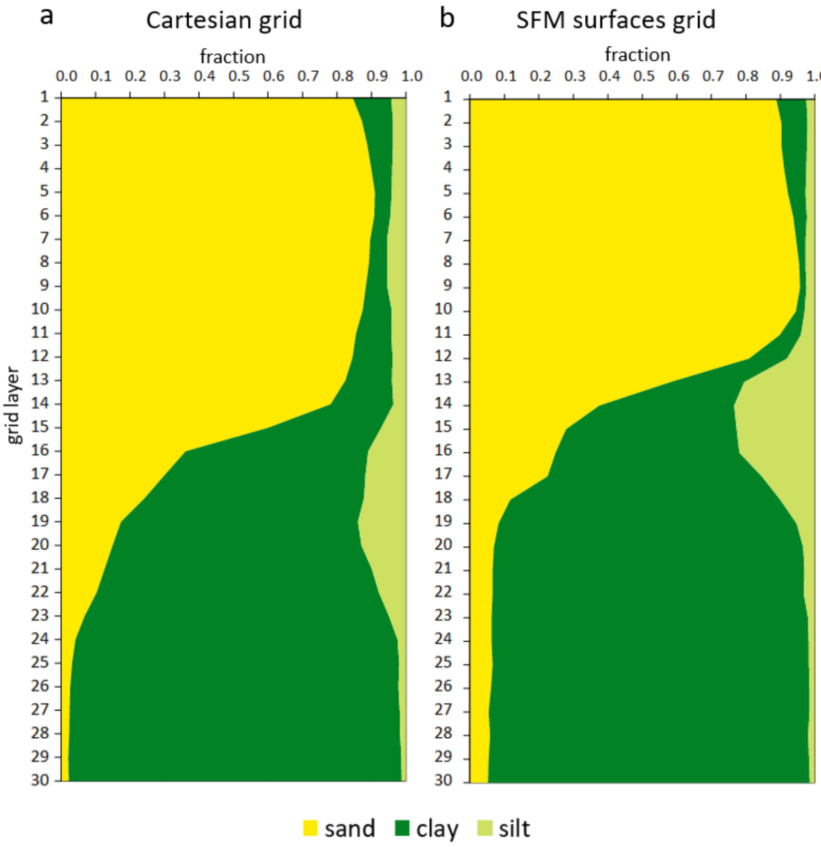


Figure 5.6. Vertical trends in fraction of the main lithofacies (sand, clay and silt) used for the lithofacies modelling.

For some of the methods that are used (Indicator Kriging (IK) and Sequential Indicator Simulation (SIS)) a variogram is required. Since the number of wells is large, it was attempted to derive an experimental variogram. However, even for the Maassluis Formation which has the largest number of wells, it was not possible to fit a variogram to the data. Therefore, the variogram settings were chosen. For IK, the simple kriging method was used and the variogram settings are 12000 m, 12000 m and 25 m in major, minor and vertical direction respectively. For SIS, the variogram settings are 5000 m, 5000 m and 10 m in major, minor and vertical direction respectively. The ranges for IK are large, because of the large well distance in some parts of the model area. If the ranges are small, areas away from the wells are assigned the most occurring lithofacies and the target lithofacies fractions cannot be achieved. For SIS, ranges need to be smaller to achieve the target fractions.

Before discussing how the SFM results can be used for the lithofacies modelling, first the results are shown when they are not used. These can later be compared to the results including information from the SFM model.

## 5.3 Lithology distribution modelling without SFM results

Two methods are used here: IK (Indicator Kriging) and SIS (Sequential Indicator Simulation). Only the cartesian grid based on the DGM surfaces will be used here, because the SFM data are not used. To account for the large difference in lithofacies between Maassluis and Oosterhout formations, they are modelled as separate zones. The fractions from the upscaled cells are used (Table 5.1 first columns), rescaled to 100% where necessary.

An example of the results is shown in Figure 5.7 for IK and in Figure 5.8 for SIS. For the chosen variogram ranges, the fractions were reproduced well for the Maassluis Formation for both methods (<2% difference between the target fraction and the simulated fraction). For the Oosterhout Formation the differences are larger: IK has 68% clay instead of the target of 64% clay and SIS has 61% clay.

Both methods show a strong influence of the wells. Patterns are not very visible except for predominantly sand in the Maassluis Formation and clay in the Oosterhout Formation. The quality of the logs in the wells has a strong influence on the results.

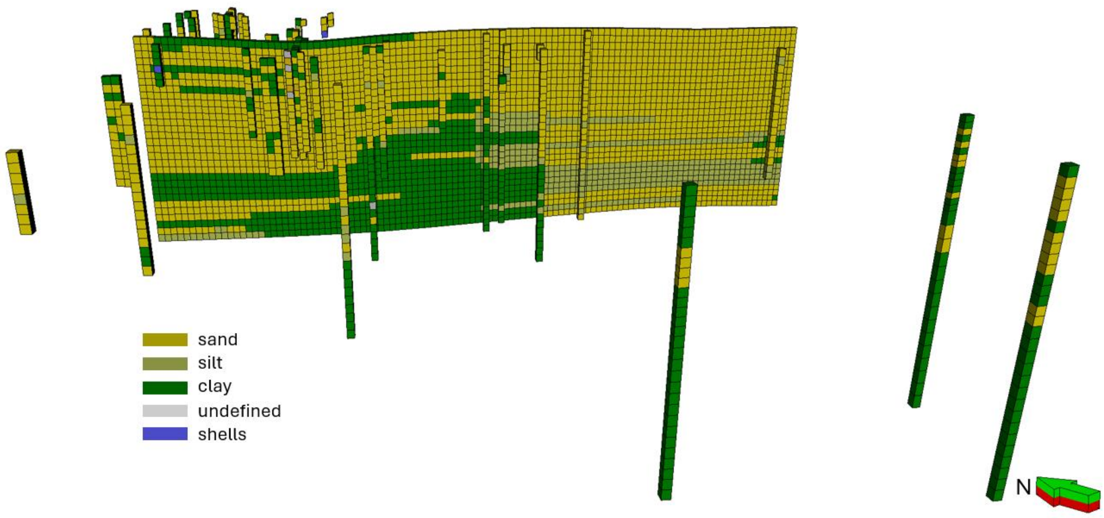


Figure 5.7 Cross-section view (from the south-west) of the lithofacies distribution simulated using indicator kriging and upscaled well logs for the model with cartesian grid. Green/red arrow indicates north. Vertical exaggeration is 25. Grid blocks are around 200 x 200 x 9 m. Length of the cross section is ~22 km.

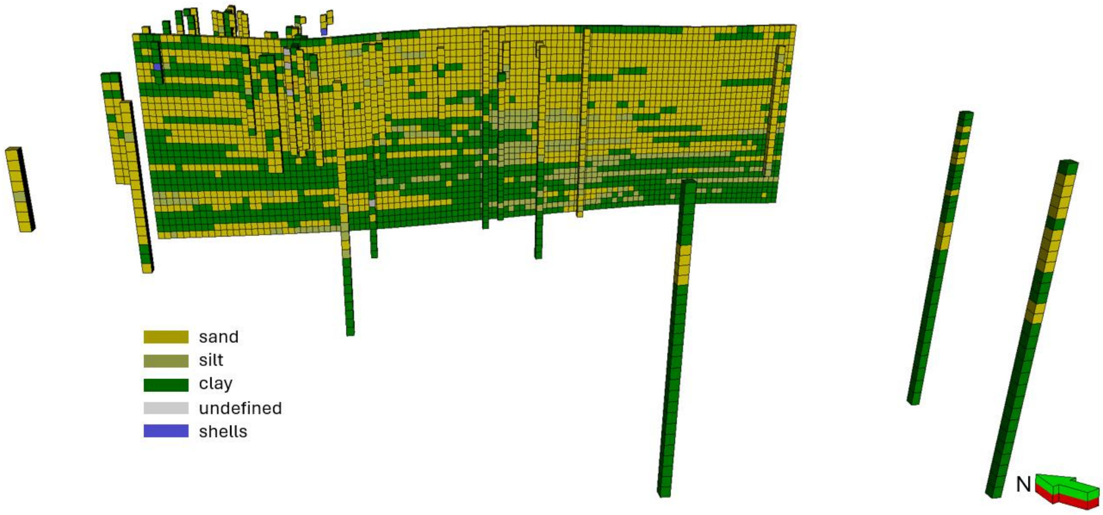


Figure 5.8 Cross-section view (from the south-west) of the lithofacies distribution simulated using Sequential Indicator Simulation and upscaled well logs for the model with cartesian grid. Green/red arrow indicates north. Vertical exaggeration is 25. Grid blocks are around 200 x 200 x 9 m. Length of the cross section is ~22 km.

## 5.4 Lithology distribution using SFM results

In this section, the SFM results will be used to simulate the lithology distribution, focusing on multiple point statistics (MPS). There are many variations possible for using MPS for generating the distribution of lithofacies. Several methods were investigated:

- The most straightforward method would be to use the SFM results directly as training image. This is not advised because of the difference in scale and size of the training image compared to the target grid. Indeed, the results of this approach were not acceptable and showed artefacts on the boundary between the lithofacies (“jagged” edges).
- A second option is to create a pattern is based on the SFM results. The pattern is subsequently used in the MPS. As for IK and SIS, the fractions of the lithofacies are specified per zone using the fractions presented in Table 5.1. Because the pattern is created on the entire model area of the SFM results, the manually applied fractions differ a lot from the fractions in the pattern. This resulted in wrong fractions of the lithofacies, like 28% sand in the Maassluis Fm instead of the target of 78%.
- A third option is to first map the SFM results to the grid on which we would like to simulate the lithofacies distribution. This can be used directly as training image. The lithofacies fractions can be defined in many ways of which two were used:
    - Per zone (Maassluis/upper and Oosterhout/lower) using the fractions presented in Table 5.1: the tolerance for achieving the lithofacies fractions is set to 1%. The training image is used as a whole instead of per zone, since the depositional framework and thus the main trends between lithofacies are the same in all zones.
    - Using the vertical trends from Figure 5.6: in this case, the zones are modelled in one go. The tolerance for achieving the lithofacies fractions is set to 2%.

The third option gave good results and the results are shown from this option. Both ways of setting the target fractions resulted in good results (i.e. within the tolerance set for achieving the fractions), except for the Oosterhout Formation in the grid based on SFM surfaces. The reason for this is probably the large discrepancy between the target fraction set (81%) and the fraction in the training image (97.5%) (see Table 5.1). This is the largest discrepancy for any of the targets. Possibly the SFM model results overestimate the clay fraction, because the upscaled well logs do show significant amounts of sand.

In Figure 5.9 and Figure 5.10 an overview is presented of the results of IK, SIS and MPS with target fractions per zone and using vertical trends. All results are constrained to the available (upscaled) well data. The results show clearly the imprint of the different methods. The IK results are very smooth and have very little variability. The SIS results have much more variability. The MPS results have intermediate results. In the MPS results the impact of the training image can be seen: silt tends to be between the sand and clay if it is present. This is not the case for the other methods. For the MPS results with a vertical trend, more detail is shown in Figure 5.11 and Figure 5.12. In these figures the impact of the trend sand-silt-clay is better visible.

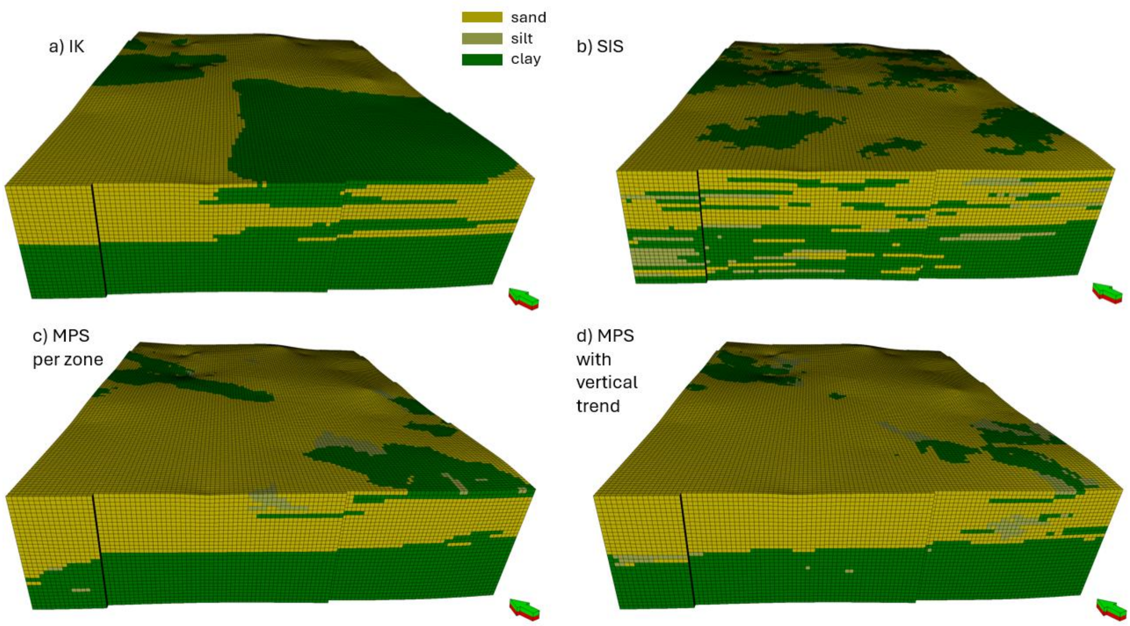


Figure 5.9. Overview of the lithology distribution in the entire model area for the cartesian grid for four methods: a) IK per zone, b) SIS per zone, c) MPS per zone and d) MPS with vertical trends.

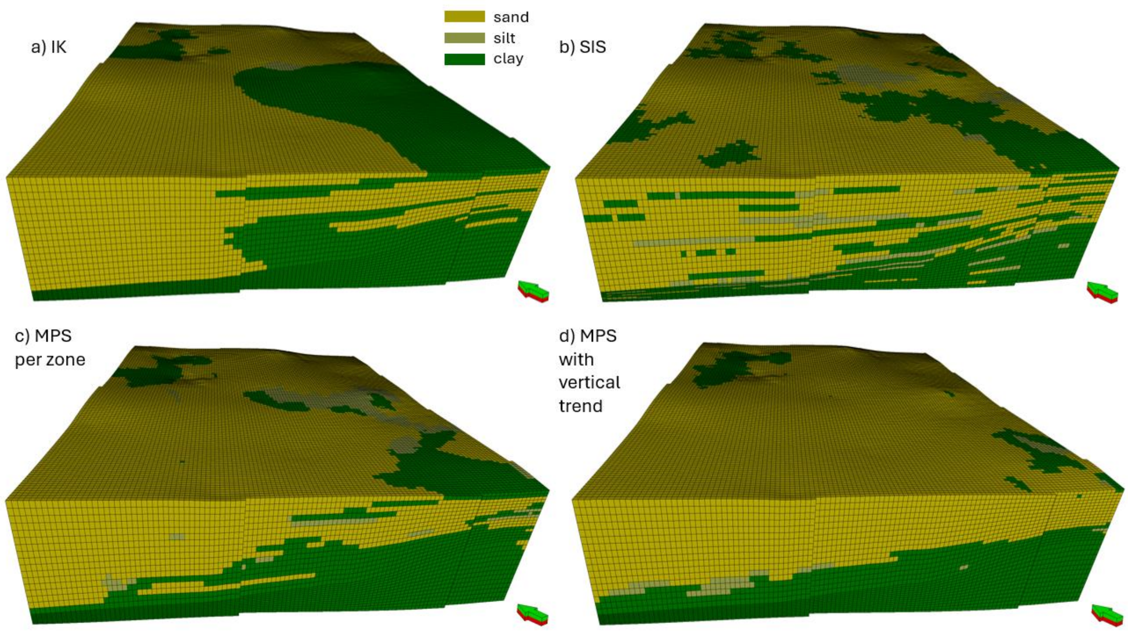


Figure 5.10. Overview of the lithology distribution in the entire model area for the grid with SFM surfaces for four methods: a) IK per zone, b) SIS per zone, c) MPS per zone and d) MPS with vertical trends.

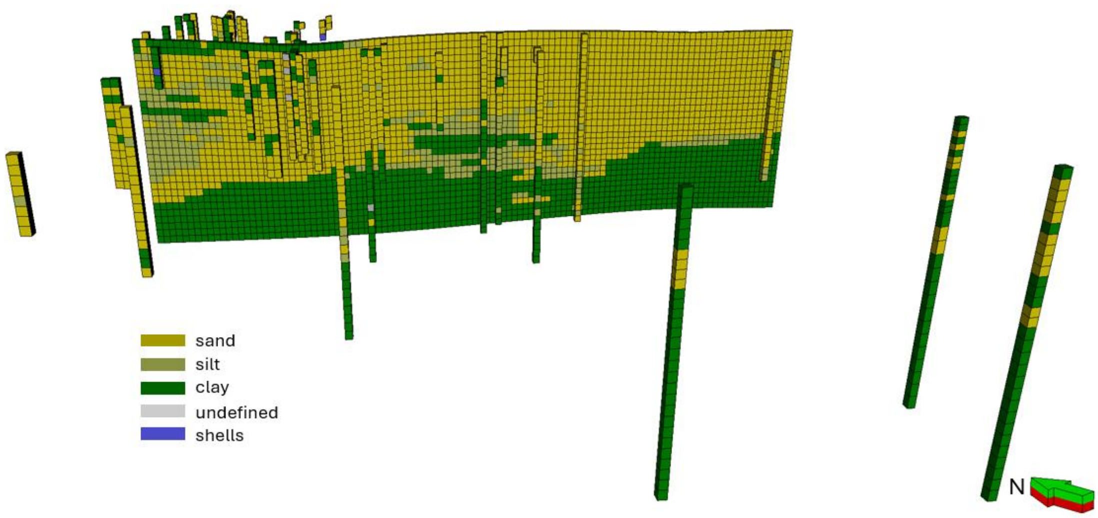


Figure 5.11 Cross-section showing the distribution of lithologies for the cartesian grid. Lithology modelled using MPS with vertical trends

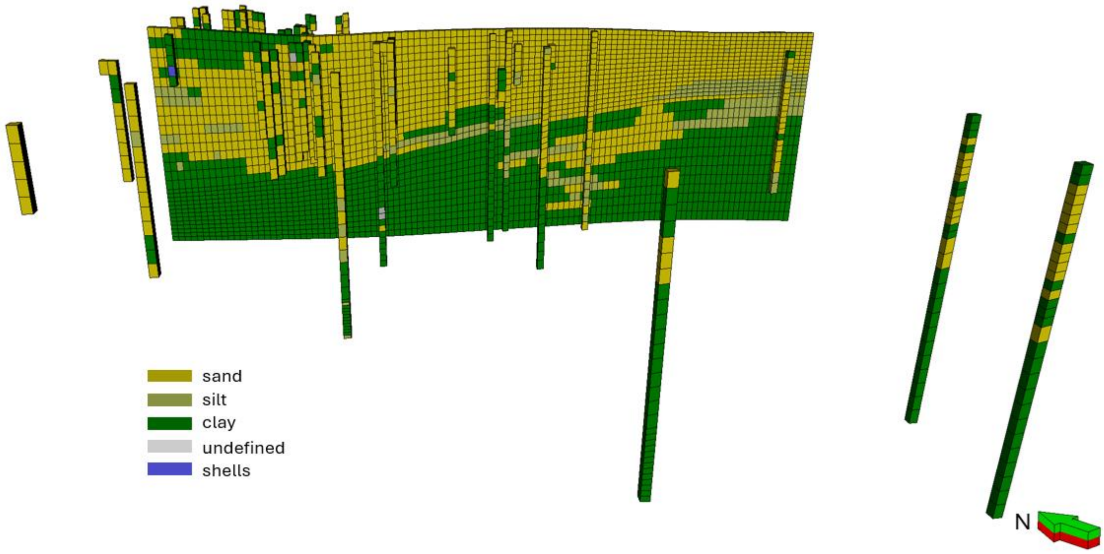


Figure 5.12. Cross section showing the distribution of lithologies for the grid with SFM surfaces. Lithology modelled using MPS with vertical trends

Since all the generated property distributions match the available well data equally well, it is difficult to quantify which property distribution is “better” or more realistic. The MPS methods represent the conceptual clinoform structures and lithofacies distribution (from sand to silt to clay) better than IK and SIS, but including the dipping structure of the layers adds this effect to the results to some extent (compare figure b of Figure 5.9 and Figure 5.10). To fit the well logs, the MPS methods also show areas where the lithofacies distribution does not fit the conceptual clinoform structure (see Figure 5.12). The variability in lithology over short distances makes it difficult for the MPS methods to apply the clinoform patterns, which are at a much coarser scale. A benefit of the SIS method is the better representation of the variability. In the IK and MPS methods, the variability appears to be smaller than that seen in the well logs. There is insufficient knowledge on the details of the depositional environment to fully understand these details and qualitatively decide which method performs better.

Another option to evaluate the results of the geostatistical methods is to compare the results to the lithofacies in the highly detailed model that was created by Veldkamp et al. (2026) for a small area (from now on referred to as the ‘Veldkamp model’). In this model, a clay layer plus underlying sand layer were mapped in the bottom part of the Maassluis Formation in an area with a high well density. The area of this model is indicated on Figure 5.1. To compare the lithofacies distributions modelled in this report to the lithofacies of the Veldkamp model, they were mapped to the grid of the Veldkamp model. Figure 5.13b-d shows the results of the SFM surfaces grid mapped to the Veldkamp model. Figure 5.13a shows the properties of the Veldkamp model: the sand layer is covered by a clay layer of around 5 m thick. The total model thickness is around 50 m. Unfortunately, none of the property simulations reproduce the main trends of the model. The regional scale model is too coarse to reproduce such detailed results. In the well log upscaling the fairly thin clay layer (~5 m) is lost in many wells (the vertical resolution of the model was ~9 m).

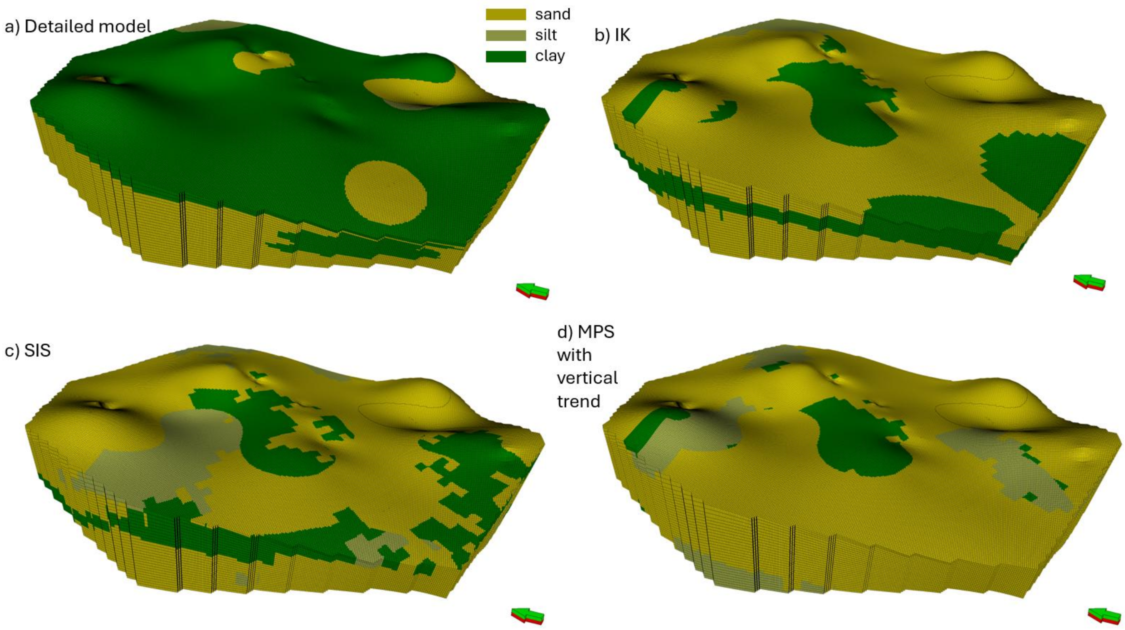


Figure 5.13. Lithofacies distribution of the three geostatistical methods (SFM surfaces grid) investigated in this chapter mapped to the detailed Veldkamp model shown in a). b) Indicator Kriging, c) Sequential Indicator Simulation and d) Multi Point Statistics with trend.

In summary the SFM results can be used in the following ways:

- Use SFM results to guide the fractions of the lithology distribution: this works best in the vertical direction. Horizontal trends are more difficult to quantify and impose. This is in particular useful in case the well data is very skewed in depth (for example many shallow and few deep wells). The SFM results provide a consistent way to correct for such a bias.
- Adding surfaces from SFM is particularly useful for flow modelling, because it enhances the lateral continuity in the right layers. These surfaces could also be derived from the mapped clinoforms, but the SFM surfaces provide a consistent set of surfaces in a larger area instead of a surface in a small area.
- SFM results can be used as a training image in MPS to improve the patterns in the lithological distribution. This is useful if patterns such as a grading from sand to silt to clay are present.

Applying MPS takes finetuning. For this case mapping the results to the target grid produced the best results. Also, the training image for MPS should be similar in scale, grid size and fractions to the target on which it is to be used. SFM is very useful in this because it is already matched to some wells.

Overall, it is concluded that the workflow used is a viable concept and improves lithology estimated based on SFM or well data only. Of course, the uncertainties in the SFM model impact the results that can be achieved by including the SFM results. However, by using it as a training image, some of the shortcomings of the SFM model, such as poorly constrained intermediate horizons, are mitigated.

## 5.5 Comparison of sand thickness maps

As for the SFM results, maps of the sand thickness were made based on the simulated lithology distributions. In this chapter, also the uncertainty of the net sand thickness is estimated.

Uncertainty of facies distributions is hard to quantify (Hadavand and Deutsch, 2017) and a full quantitative estimation of the uncertainty is beyond the scope of this project.

For reservoir properties a standard way of quantifying the uncertainty is by simulating a large number of realisations with the appropriate statistical characteristics. This works well if wells are distributed over the entire model area, but in areas away from wells the properties will converge to the statistical properties that have been specified. For lithofacies simulation in areas away from wells, the lithofacies fractions are reproduced and the uncertainty reduces to (almost) zero for the MPS-methods and to a fixed value based on the lithofacies fractions for SIS. So, the uncertainty in the lithofacies fractions needs to be included in a proper description of the uncertainty, for example via the method suggested by (Hadavand and Deutsch, 2017). In addition, the uncertainty in the lithology interpretation in the wells should be included. Since this is beyond the scope of this work, a simplified approach to get a qualitative estimate of the uncertainty is used, assuming that at a large distance from any wells the uncertainty is the highest. The steps are as follows:

- Create multiple (100 in this case) realisations of the lithology distribution.
- From the realisations, calculate per grid block the fraction $f_{i,j,k}$ of the realisations that has sand.
- Calculate per zone the expected sand thickness per column ($Hs_{i,j}$) from the fractions and the gridblock height H:

$$Hs_{i,j} = \sum_{k=1}^{n} f_{i,j,k} H_{i,j,k}$$

- Estimate the uncertainty $U_{i,j,k}$ per cell as:

$$U_{i,j,k} = \begin{cases} f_{i,j,k}, & f < 0.5 \\ 1 - f_{i,j,k}, & f \geq 0.5 \end{cases}$$

- Create a property that specifies if a gridblock is within the range of a well or not (considering the depth of wells) (horizontal direction up to 1 km, vertical is 5 m)
- Set the uncertainty everywhere outside of the range to the maximum value (0.5)
- Estimate per zone and per column, the grid block height-weighted average of the uncertainty $Us_{i,j}$:

$$Us_{i,j} = \sum_{k=1}^{n} U_{i,j,k} H_{i,j,k} \Big/ \sum_{k=1}^{n} H_{i,j,k}$$

The average and uncertainty of the sand thickness are calculated for two methods (SIS with manually set fractions as in Table 5.1 and MPS with vertical trend in Figure 5.6) and for the two grids (Cartesian grid and SFM surfaces grid). For the Cartesian grid, the results are reported for the Maassluis and Oosterhout formations as defined in DGM and for the SFM surfaces grid for the upper (sandy) and lower (clayey) zone.

Figure 5.14 and Figure 5.15 show the sand thickness maps for the DGM Maassluis and Oosterhout formations respectively for the cartesian grid and with lithofacies simulated using MPS with vertical trend. In the figure marked with b the qualitative uncertainty is presented. The figures for the other grids and methods are presented in Appendix C. The main observations are as follows:

About the methods:

- The sand thickness of the MPS method with vertical trends is higher in the upper part because the fraction of sand was set higher.
- SIS results in higher uncertainty than MPS.

About the results:

- The sand thickness ranges from 40 to 150 m in the Maassluis Formation and 70 to 190 m for the upper zone defined using SFM. In the Oosterhout Formation/lower zone the range of the sand thickness is 0 to 70 m.
- For the SFM surfaces grid, the sand thickness decreases from south-east to north-west which is largely caused by the change in thickness of the zone. This change in thickness is visible in Figure 5.12.
- The uncertainty (shown on the b-side of Figure 5.14, Figure 5.15 and the figures in Appendix C) is lower in the Maassluis Formation/upper zone than in the Oosterhout Formation/lower zone, because the number of wells decreases with depth.
- In the Maassluis/upper zone, the deep well WAS-05 causes a bulls-eye showing much more clay than any of the other wells in the area. The well has a spontaneous potential-log only (Veldkamp et al., 2026) and the results could well be uncertain due to that. In this depth zone, the resistivity is estimated to change significantly and errors in the trend could cause problems in the interpretation.
- In the low zone for the SFM surfaces grid, almost all wells have low uncertainty and no sand in the MPS results (Figure C.) and no to 20 m sand in the SIS results (Figure C.). This suggests that in this depth range little sand occurs in the entire model area. Only well PNA-GT-04 (see Figure 1.1 and Figure 5.14 for well locations) causes a very distinctive bull's eye in the results for the Oosterhout/lower layer. This is very visible in the SFM surfaces grid for MPS with vertical trend (Figure C.). Review of this well showed that the well has only a GR (gamma ray) log and the interpretation depends strongly on the selected cut-off (Veldkamp et al., 2026). It could be that the cut-off is not selected optimally and that the well has clay like all the other wells in this zone. It should be noted however that at a depth of ~260 m, a distinctive layer occurs that has very low GR and that nearby well B37E3633 also shows high sand content up to a depth of 220 m.
- For the DGM Oosterhout Formation, the highest probability of encountering sandy layers is in the north-west, but the uncertainty is high. In the SFM surfaces grid, which has dipping layers, most of this sand is part of the upper zone except for a sandy layer in two wells (LED-03 and WAS-05) in the most northern tip of the model area. The layer occurs at a depth of 310 m in LED-03 and at 350 m in WAS-05 and could be correlated given the dip of the SFM surface in the area.

Although both the sand thickness maps and uncertainty estimates still carries considerable uncertainty, the sand thickness maps present a useful addition to the current REGIS interpretation and can help to identify areas were both the sand and clay layers are present which would allow development of HT-ATES systems. In the north-western part of the model area, the Maassluis Formation also shows some more clayey parts at the top of the formation, which could serve as the required seal for HT-ATES. In the same area, the Oosterhout Formation has some sandy layers at the top of the formation, which could potentially be interesting. In the southern part of the model area (in the direction of Botlek), the sand thickness is estimated to be lower. In this area, the Maassluis Formation is more clayey and clay layers could be more laterally extensive. Detailed local studies are required to confirm these interpretations.

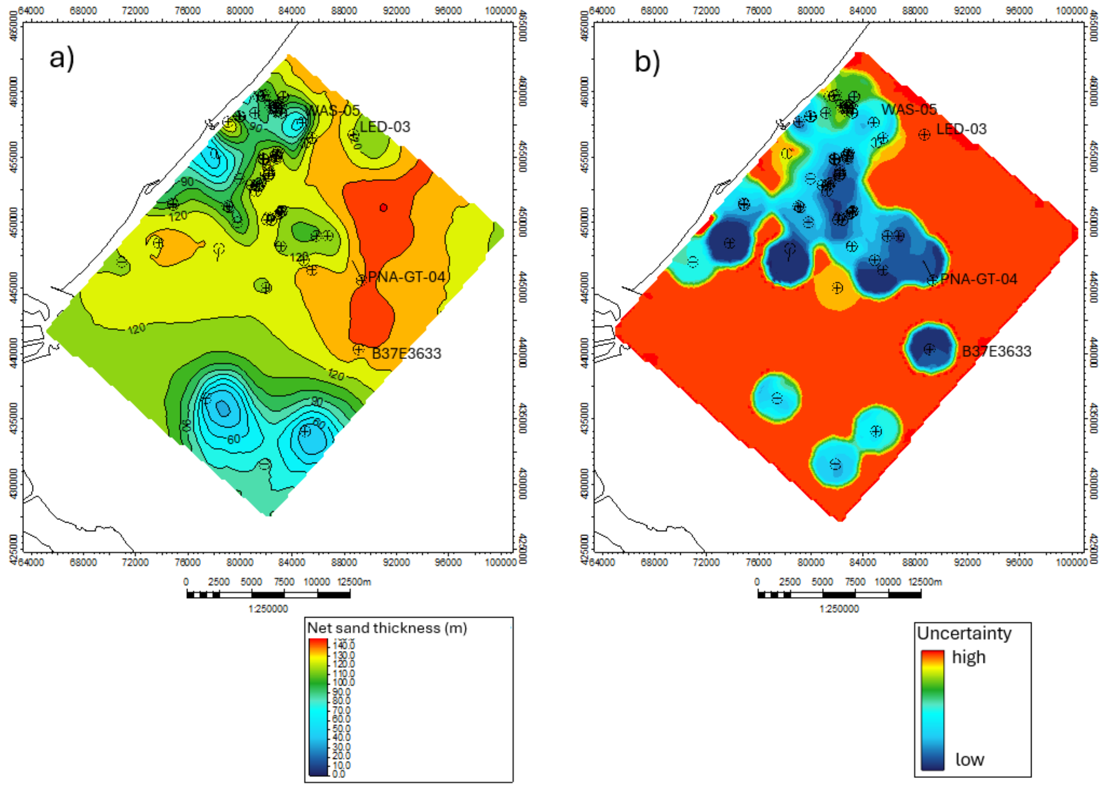


Figure 5.14 Sand thickness (a) and qualitative uncertainty in the sand thickness (b) of the DGM Maassluis Formation for the cartesian grid with the lithology simulated using MPS with vertical trend.

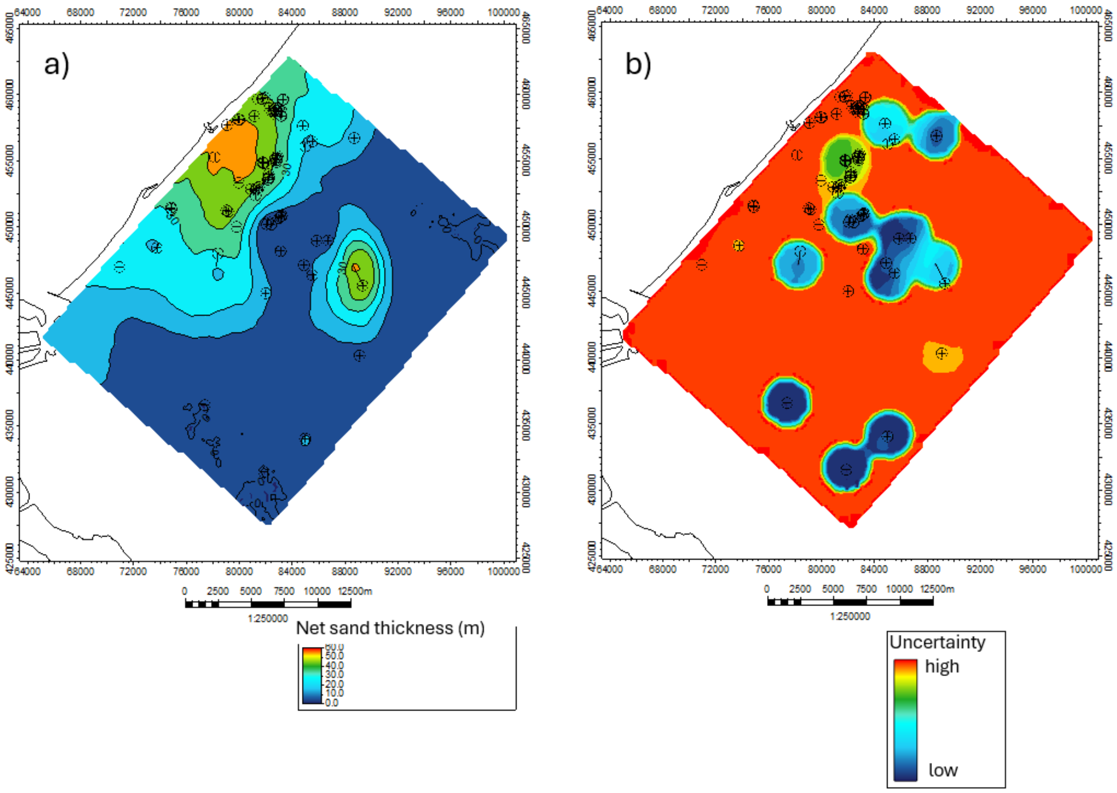


Figure 5.15 Sand thickness (a) and qualitative uncertainty in the sand thickness (b) of the DGM Oosterhout Formation for the cartesian grid with the lithology simulated using MPS with vertical trend.

# 6 Discussion

The SFM made in this study is a first attempt to create a more realistic subsurface model for the Oosterhout and Maassluis formations in the region of South-Holland than the current division in sand and clay units in REGIS II. In this first attempt, the focus was on establishing an optimal fit of lithofacies and depth markers of the model with the selected boreholes. Magnitudes of sediment supply of 4500 $km^3$/Ma and water discharge 4700 $m^3$/s have been suggested based on recent analogue comparison and recent Rhine-Meuse river sediment load and water discharge (Middelkoop et al., 2010). However, for our model to fit with the well data horizon markers, we had to use values of less than 25% of these values from literature. As our model is a regional-scale model (not covering the entire Netherlands), different values for sediment supply and fluvial discharge can occur. In our model the clinoforms are mainly driven by a prograding river/delta system. However, another potentially important sediment source in the model, namely longshore currents could be a major sediment redistribution factor along the coastal system (which is currently not included in the model).

For now, the paleobathymetry was determined based on the interpreted clinoform heights only for the base Oosterhout using the method of Hijma et al. (2025). However, we do not know what parts of these structures have been eroded after deposition. In this study, we kept the paleobathymetry constant through time as we did not have clear arguments for the paleobathymetry of the clinoform horizons. The paleobathymetry is a key parameter in controlling accommodation space creation in the system. Therefore, information on the paleobathymetry through time should be constrained for the deposition of these clinoforms, but within this study time did not allow for this.

**Clinoform structures**

Progradational clinoforms are typically characterized by a vertical coarsening-upward signature (Figure 6.1). They are expected to form due to an increase in energy in the depositional environments from the prodelta to the shoreface because of system dynamics along the coastline (Figure 6.1). Our SFM results reflect two-step infilling, where: 1) by Pliocene times sediment accumulation paces with the infill of isolated depressions, which are the result of a subaqueous system, 2) at the base of the Pleistocene we see a major increase in sediment supply that leads to the large-scale clinoform geometries, which due to progressive progradation is coarsening-upward (Figure 4.3b-d). Further biostratigraphic evaluation is required to place these processes in time.

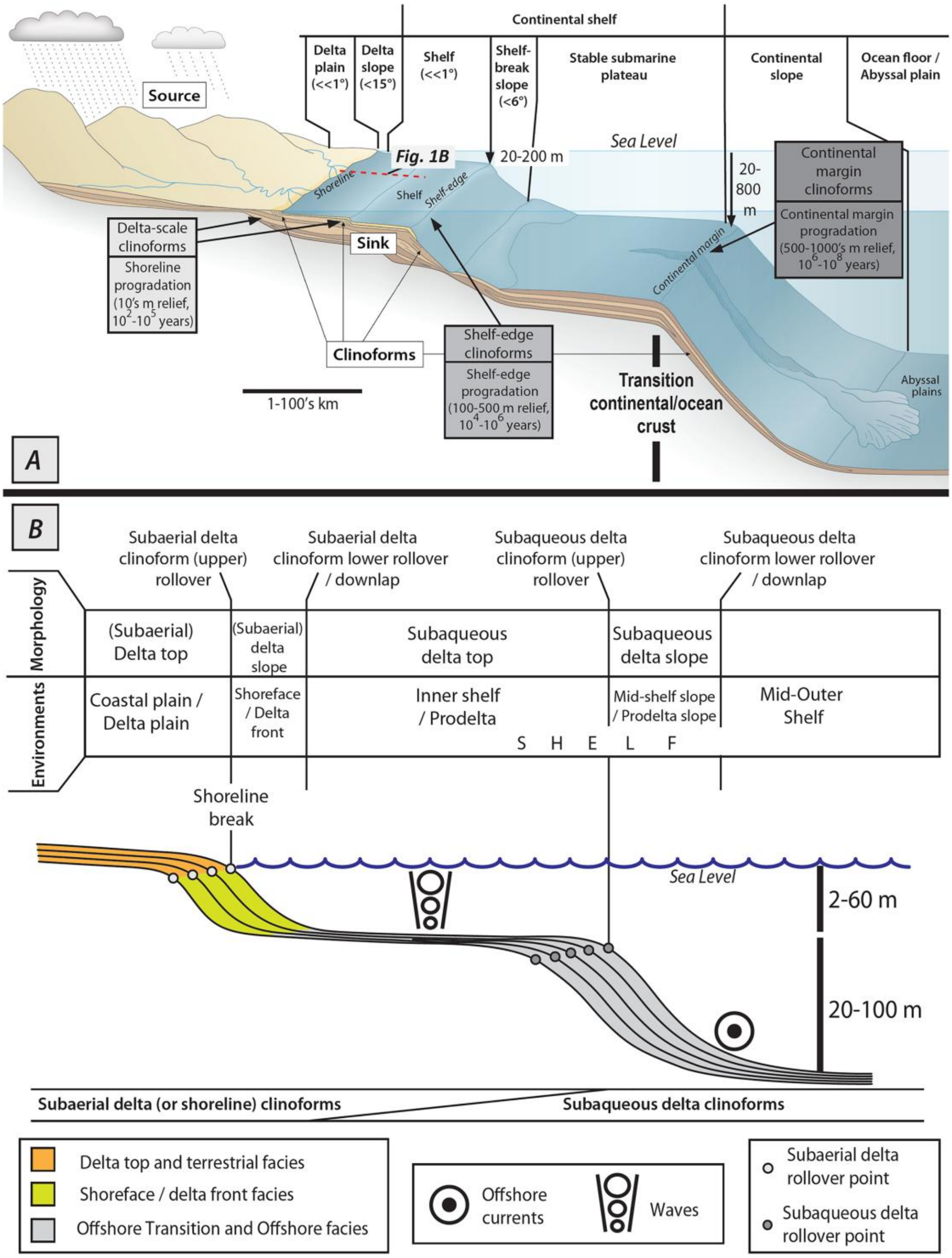


Figure 6.1 Cross-sectional view showing idealized compound clinoform systems at different scales. (A) Regional cross-section, highlighting three actively growing clinoforms systems: delta, shelf-edge and continental-margin scale clinoforms. (B) Cross-section through the nearshore to inner marine shelf area, showing a typical shoreline to delta-scale subaqueous clinoform compound system (Patruno & Helland-Hansen, 2018)

The distribution of the lithofacies in the clinoforms also affects the flow. In the idealised case above, a sandy layer develops at the top which overlies the finer sediments. Although this sandy layer can be horizontal, the continuity is poor due to the clinoform structures. The surface mapped in the seismic data, is also not a good indication of a flow unit, because the particle size decreases downslope. Representing the details of the lithofacies distribution correctly is therefore important to understand the permeability distribution.

# 7 Conclusions and recommendations

In this report a first attempt was made to simulate the deposition in the region of Zuid-Holland in the Oosterhout and Maassluis Formations using stratigraphic forward modelling (SFM) and use the SFM results to improve modelling of the lithology distribution in smaller scale models using geostatistical methods. The workflow was successfully demonstrated and maps of sand thickness at regional scale (tens of kilometers) were produced which were constrained to lithology observed in wells and to SFM results. At the local scale, the current SFM results are too coarse to be used. The geostatistically simulated regional scale lithofacies are also too coarse to predict detailed lithology distributions at the local scale.

To further enhance the SFM models that were constructed during this study it is recommended to add more well data covering a larger part of the model area, and more seismic interpretations if available. This allows for a better comparison between wells and a better representation of sand/clay lateral distribution in the model. Within this study we could also clarify what the main drivers are in the sedimentary system, which are in a first instance: paleobathymetry, sea level, and sedimentary source position, supply and discharge. In a next step, it will be important to perform sensitivity analysis on these parameters to analyse how the modelled values from this study compare to the conceptual knowledge, and to change them accordingly to obtain an optimized geologically coherent reservoir model.

Additionally, better age constraints for the intermediate clinoform structures should be determined. Also, extrapolation of these intermediate horizons should be done conform an overall structural trend or additional seismic interpretation studies. Also, better constraints on the sedimentation rate in these clinoforms and how these rates vary from deep to shallow marine environments would help to optimize the forward model. Specifications on the type of clinoforms and their coastal system and post depositional erosional events should be checked.

Within this study a generalized sea level curve is used and a constant paleobathymetry through time. However, these two parameters have a major impact on the sedimentary system. By obtaining more information on these parameters for the study area a better representation and understanding of the coastline position, amount of erosion in the system and the sediment supply can be obtained.

A CougarFlow uncertainty, sensitivity and risk analysis could be performed to further assess the effect of uncertain parameters on the modeling results. An SFM model honors observations using geological processes, but it is not necessarily the only result that does so. Other SFM realization of the same model with different input parameters might refine the model fit to the field observations. This would result in a different interpolation between data points, which can be done by performing an uncertainty, sensitivity and risk analysis.

Because the MPS training image created using the SFM results is quite coarse and only shows a large scale trend of sand to silt to clay, it is difficult to simulate the local variability that is observed in the wells. It is recommended to test whether adding sand classes in the SFM output can help to create more detailed training images. If this doesn't work, it is recommended to investigate other ways to improve the variability and level of detail in the training image.

In the workflow used in this study, shallow and deep wells were combined which typically have different data. In addition to good quality control of the well data, which is always important, it is necessary to ensure that the data from the two sources is consistent. From the maps, it appears that the well logs interpretations of the deep well, can be quite different from nearby shallow wells. In the shallow wells, descriptions are sometimes not in line with available logs. But these differences appear to be random, rather than the bias seen in the deep wells. It should be further investigated how the different data types can be interpreted to ensure consistent data.

# References

Altenburg, R., & van Unen, M., 2025. Towards national mapping of the Breda Subgroup and Oosterhout Formation. Utrecht: TNO. WarmingUP*GOO* report. https://www.warmingup.info/documenten/reportwupgoo_mappingbredaoo_final.pdf

Busschers, F., Cohen, K., Wesselingh, F., Bakker, M., Schokker, J., van Balen, R., & van Heteren, S., 2025. Quaternary. In *Geology of the Netherlands* (pp. 333-391). Routledge.

Dearing Crampton-Flood, Emily, et al., 2020. A new age model for the Pliocene of the southern North Sea basin: a multi-proxy climate reconstruction. *Climate of the Past* 16.2: 523-541

Deutsch, C.V. & A.G. Journel, 1998. GSLIB geostatistical Software Library and User's Guide, 2nd Edition. (www.gslib.com)

Ducros, M., Steffens, L. M., de Souza Brugognolle, J., Boing, J. V. L., Soares, A. P., & Bettú, D. F., 2023. A new objective function designed for the calibration of stratigraphic forward models. Marine and Petroleum Geology, 154, 106306

Hawie, N., Barrois, A., Marfisi, E, Murat, B., Hall, J., El Wazir, Z., Al-Madani, N., & Aillud, G., 2015. SPE-177519-MS Forward Stratigraphic Modelling, Deterministic Approach to Improve Carbonate Heterogeneity Prediction; Lower Cretaceous, Abu Dhabi. Doi: 10.2118/177519-MS.

Hadavand, M and C.V. Deutch, 2017. Facies proportion uncertainty in presence of a trend. J. of Petroleum Science and Engineering 153. P 59-69. dx.doi.org/10.1016/j.petrol.2017.03.036

Hijma, M.P., Bradley, S.L., Cohen, K.M. et al, 2025. Global sea-level rise in the early Holocene revealed from North Sea peats. Nature 639, 652–657. https://doi.org/10.1038/s41586-025-08769-7

Kombrink, H., Doornenbal, J.C., Duin, E.J.T., den Dulk, M., van Gessel, S.F., ten Veen, J.H., & Witmans, N., 2012. New insights into the geological structure of the Netherlands; results of a detailed mapping project. Netherlands Journal of Geosciences, 91-4, 419-446.

Kuhlmann, G., 2004. High resolution stratigraphy and paleoenvironmental changes in the southern North Sea during the Neogene: An integrated study of Late Cenozoic marine deposits from the northern part of the Dutch offshore area. UU repository

Lisiecki, L. E., & Raymo, M. E., 2005. A Pliocene-Pleistocene stack of 57 globally distributed benthic δ18O records. *Paleoceanography*, *20*(1).

Middelkoop, H., Erkens, G. & van der Perk, M., 2010. The Rhine delta—a record of sediment trapping over time scales from millennia to decades. J Soils Sediments 10, 628–639. Doi: 10.1007/s11368-010-0237-z

Noorbergen, L. J., Lourens, L. J., Munsterman, D. K., & Verreussel, R. M. C. H., 2015. Stable isotope stratigraphy of the early Quaternary of borehole Noordwijk, southern North Sea. *Quaternary International*, *386*, 148-157.

Overeem,I., Weltje,G.J., Bishop-Kay, C., & Kroonenberg, S.B., 2002. The Late Cenozoic Eridanos delta system in the Southern North Sea Basin: a climate signal in sediment supply? Basin research, 13, 293-312

Patruno, S., & Helland-Hansen, W., 2018. Clinoforms and clinoform systems: Review and dynamic classification scheme for shorelines, subaqueous deltas, shelf edges and continental margins. Earth-Science Reviews, 185, 202-233. https://doi.org/10.1016/j.earscirev.2018.05.016.

Pluymaekers, M. P. D., van Wees, J. D. A. M., van der Kuip, M., & Vandeweijer, V., 2013. Hoge temperatuur opslag in de ondiepe ondergrond (Report nr. R11694). Dutch Institute for Applied Geosciences, TNO. Retrieved from the website: http://www.kennisplatformbodemenergie.nl/wp-content/uploads/2016/03/HTO-Hoge-temperatuuropslag-in-de-ondiepe-ondergrond.pdf

Rohling, E. J., Foster, G. L., Gernon, T. M., Grant, K. M., Heslop, D., Hibbert, F. D., et al., 2022. Comparison and synthesis of sea-level and deep-sea temperature variations over the past 40 million years. *Reviews of Geophysics*, *60*, e2022RG000775. https://doi.org/10.1029/2022RG000775

Strebelle, S. (2002) Conditional simulation of complex geological structures using multiple-point statistics. Mathematical Geology, 34, p. 1-22.

TNO – GDN (2021) BRO DGM v2.2 TNO - Geological Survey of the Netherlands, https://www.dinoloket.nl/en/subsurface-models/map; visited 2021-11-25

Veldkamp, J.G., Peters, E. Dinkelman, D., van Huizen, J. P., Spekreijse, P., Jorissen, M.J. & Bouwmeester, 2026. Characterization and HT ATES potential estimation in the The Hague region of Zuid-Holland. WarmingUP GOO report, WP 1.2

# Appendix A Clinoform geometries

Activities as part of the Warming[UP]*GOO* project include national scale seismic interpretation and mapping of the top and base of the Oosterhout Formation (Altenburg and van Unen, 2025; see also Figure 3.2). On only a small part (about five) of these interpreted SCAN seismic lines clinoform structures could be observed. From these interpretations, an average of 13.5% of the clinoform heights with respect to the total depth of the base Oosterhout was obtained (Figure A.1, Figure A.2 and Figure A.3).

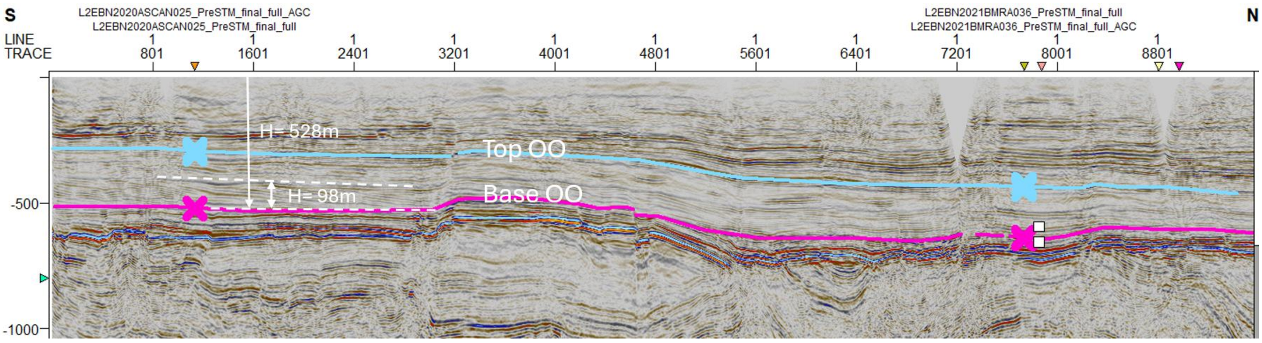


Figure A.1 SCAN line 026 clinoform height of 98 m and depth to base Oosterhout formation of 528 m. This gives a percentage of 18.5% of the clinoform height with respect to the depth of the Oosterhout Formation (See Figure 3.2 for the location of the seismic line).

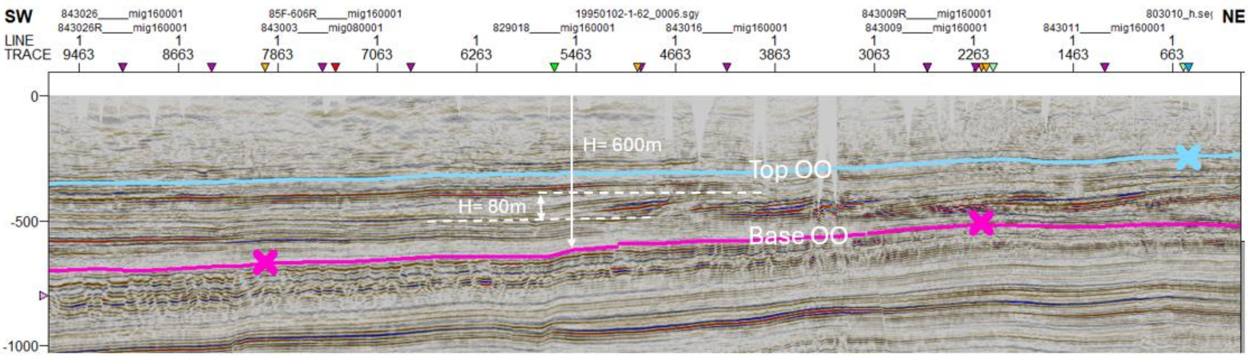


Figure A.2 SCAN line 035 clinoform height of 80 m and depth to base Oosterhout formation of 600 m. This gives a percentage of 13% of the clinoform height with respect to the depth of the Oosterhout Formation (See Figure 3.2 for the location of the seismic line).

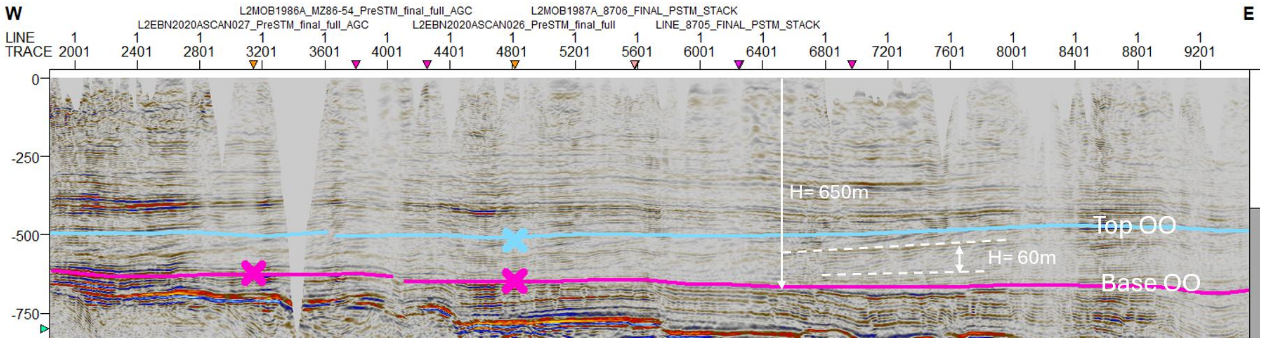


Figure A.3 SCAN line 037 clinoform height of 60 m and depth to base Oosterhout formation of 650 m. This gives a percentage of 9% of the clinoform height with respect to the depth of the Oosterhout Formation (See Figure 3.2 for the location of the seismic line).

# Appendix B List of wells (chapter 5)

| Well name | well head x coordinate | well head y coordinate | TD (TVDSS) |
|---|---|---|---|
| B30D0217 | 78140 | 455360 | 158.4 |
| B30G0500 | 82790 | 454990 | 135.3 |
| B30G0742 | 83312 | 459716 | 152 |
| B30G0743 | 83169 | 458458 | 154 |
| B30G0779 | 81120 | 458450 | 144.7 |
| B30G0780 | 81400 | 459730 | 145.1 |
| B30G0821 | 82963 | 459036 | 145.6 |
| B30G0822 | 82793 | 458848 | 146.8 |
| B30G0823 | 82790 | 458865 | 147.1 |
| B30G0825 | 82725 | 458982 | 147 |
| B30G0827 | 82712 | 458997 | 148.3 |
| B30G0828 | 82698 | 459015 | 147.9 |
| B30G0830 | 82256 | 459048 | 147.5 |
| B30G0833 | 82770 | 458815 | 146.6 |
| B30G0877 | 84975 | 456175 | 142.9 |
| B30G0936 | 85500 | 456540 | 135.5 |
| B30G0970 | 81213 | 452467 | 253 |
| B30G1101 | 83192 | 458801 | 148.6 |
| B37B0172 | 70930 | 447060 | 162 |
| B37E0481 | 83130 | 448250 | 200.5 |
| B37E0483 | 83100 | 448270 | 194.7 |
| B37E0510 | 82000 | 445080 | 125.7 |
| B37E0581 | 85500 | 446450 | 120.9 |
| B30G7866 Jan Brouwer | 82401 | 450267 | 280 |
| B30D1775 | 79778 | 450097 | 232.9 |
| B30D1776 | 79942 | 453429 | 226.1 |
| B30G0025 | 81940 | 459840 | 146.5 |
| B30G0041 | 83270 | 459670 | 169.7 |
| B30G0188 | 82430 | 458850 | 148.4 |
| B30G0189 | 82720 | 458570 | 129.2 |
| B30G0608 | 83135 | 458475 | 138.6 |
| B30G0612 | 81730 | 459780 | 115 |
| B37B0049 | 73760 | 448520 | 262.1 |
| B37E0001 | 84870 | 447200 | 142.1 |
| B37E3633 | 89077 | 440382 | 251.8 |
| B37E6785 Delftse Hout (DAPGEO-2 500 m well) | 85833 | 449052 | 205.8 |
| B37G0443 | 81857 | 431608 | 446.1 |
| B37G0442 PRW-OBS | 84978 | 434126 | 444.1 |

| | | | |
|---|---|---|---|
| B37D0228 MAS-OBS | 77387 | 436644 | 446.3 |
| KHL-GT-02 | 78263 | 447047 | 2472.7 |
| LED-03 | 88667 | 456781 | 1168.7 |
| PNA-12 | 86703 | 449181 | 1877.5 |
| PNA-GT-04 | 88619 | 447064 | 2342.1 |
| WAS-05 | 84799 | 457730 | 1334.7 |
| DEL-GT-01 (top 500 m) | 85106.35 | 446165.3 | |
| Centre Court (K) | 82877 | 455441 | 237.7 |
| Centre Court (W) | 82827 | 455277 | 254.7 |
| Deo_Gratias (K1) | 80002 | 458176 | 237 |
| Deo_Gratias (W1 B30D7265) | 79907.73 | 458215.7 | 235 |
| European Patent Office (K1) | 83093 | 450856 | 208 |
| European Patent Office (K2) | 83118 | 450877 | 210 |
| European Patent Office (W1) | 82986 | 450761 | 209 |
| European Patent Office (W2) | 83195 | 450947 | 210 |
| Gemeentekantoor Fruitweg 17 (B30G7773) | 80870 | 452950 | 253.7 |
| Haagse Hogeschool (K1) | 82182 | 453685 | 250 |
| Haagse Hogeschool (K2) | 82159 | 453670 | 252 |
| Haagse Hogeschool (K3) | 82136 | 453655 | 252 |
| Haagse Hogeschool (W1) | 82230.02 | 453805.4 | 253 |
| Haagse Hogeschool (W2) | 82211.3 | 453811.8 | 269 |
| Haagse Hogeschool (W3) | 82190.56 | 453818.8 | 269 |
| Hoogvliet (mono) | 79064 | 457774 | 236 |
| Monarch (K) | 82802 | 455135 | 241 |
| Monarch (W) | 82694.78 | 455230.3 | 234 |
| Parnassia (K) | 74825 | 451539 | 217 |
| Parnassia (W) | 74862 | 451439 | 214.5 |
| Spuikwartier K1 | 81751.4 | 454941.7 | 280 |
| Spuikwartier K2 | 81780.21 | 454968 | 292 |
| Spuikwartier W1 | 81823.66 | 454885.2 | 285 |
| Spuikwartier W2 | 81832.41 | 454907.6 | 284 |
| Stadsdeelkantoor Escamp Leyweg K1 | 79148 | 451251 | 250 |
| Stadsdeelkantoor Escamp Leyweg W1 | 79016 | 451341 | 245 |
| Stationspostgebouw (W1) | 82206.75 | 454060.1 | 265 |
| Waldo City (mono) | 81214 | 452873 | 248.8 |
| Waldo Mountains (K) | 81459 | 453087 | 269.7 |
| Waldo Mountains (W) | 81338 | 452980 | 269 |
| B30G4529 | 82150 | 450480 | 386.7 |
| B30G4529 new logs | 82150 | 450480 | 386.7 |
| B30G0935 (Shell 2000) | 82150 | 450480 | 431 |
| DaVinci (2010) | 82056 | 450300 | 219 |

# Appendix C Maps of sand thickness

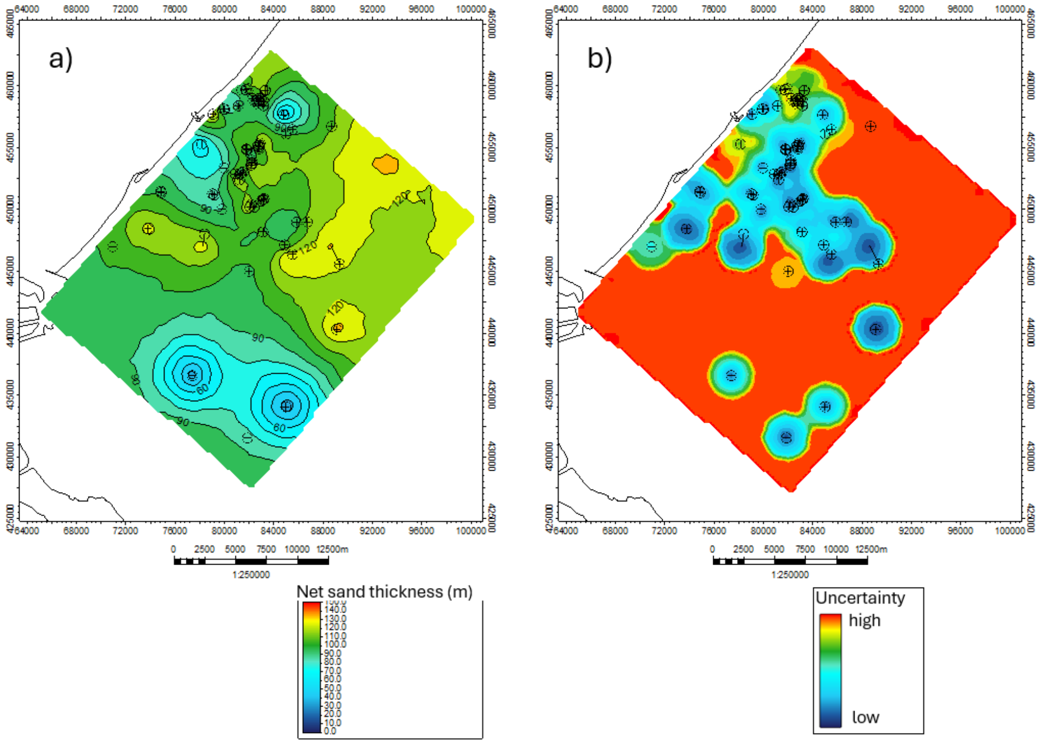


Figure C.1 Sand thickness (a) and qualitative uncertainty in the sand thickness (b) of the DGM Maassluis Formation for the cartesian grid with the lithology simulated using SIS with manually set lithology fractions.

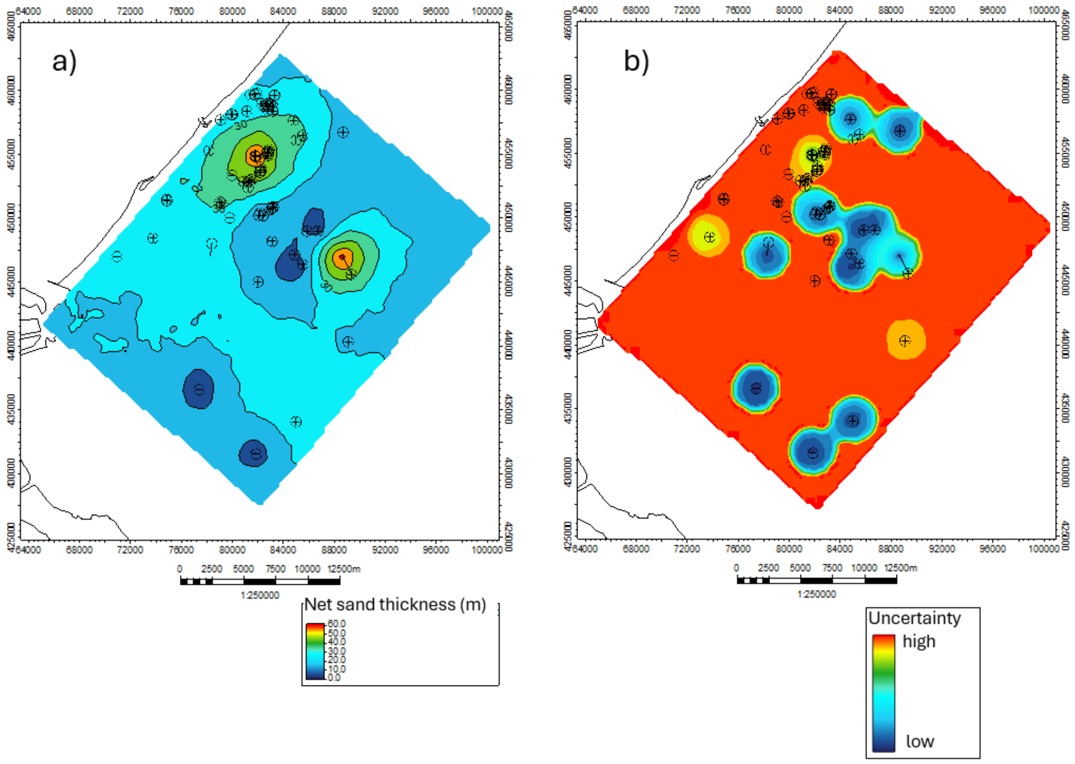


Figure C.2 Sand thickness (a) and qualitative uncertainty in the sand thickness (b) of the DGM Oosterhout Formation for the cartesian grid with the lithology simulated using SIS with manually set lithology fractions.

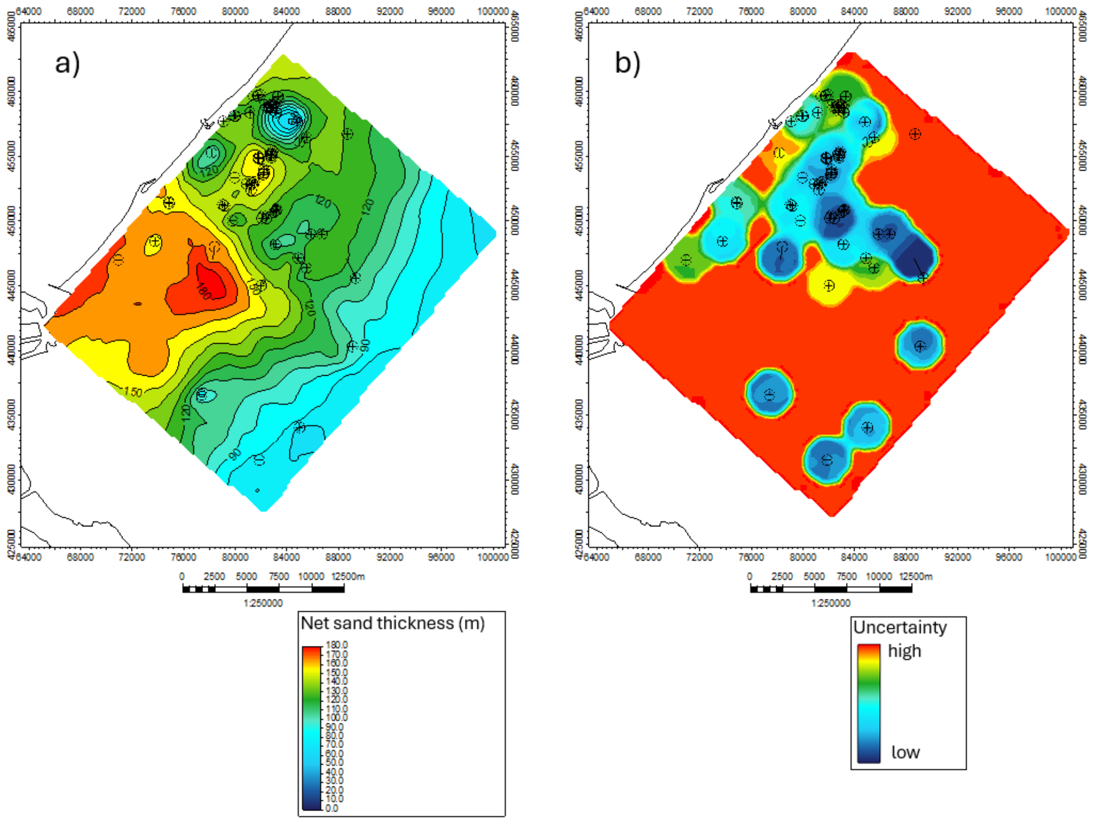


Figure C.3 Sand thickness (a) and qualitative uncertainty in the sand thickness (b) of the upper zone of the SFM surfaces grid with the lithology simulated using MPS with vertical trend.

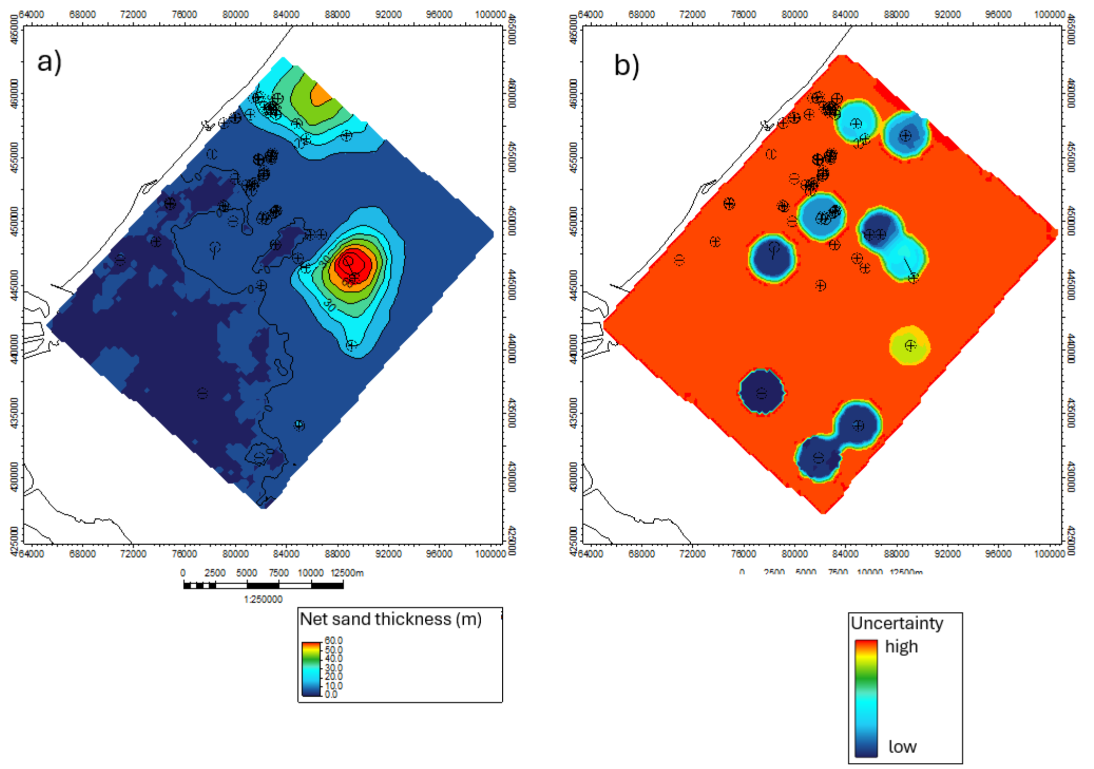


Figure C.4 Sand thickness (a) and qualitative uncertainty in the sand thickness (b) of the lower zone of the SFM surfaces grid with the lithology simulated using MPS with vertical trend.

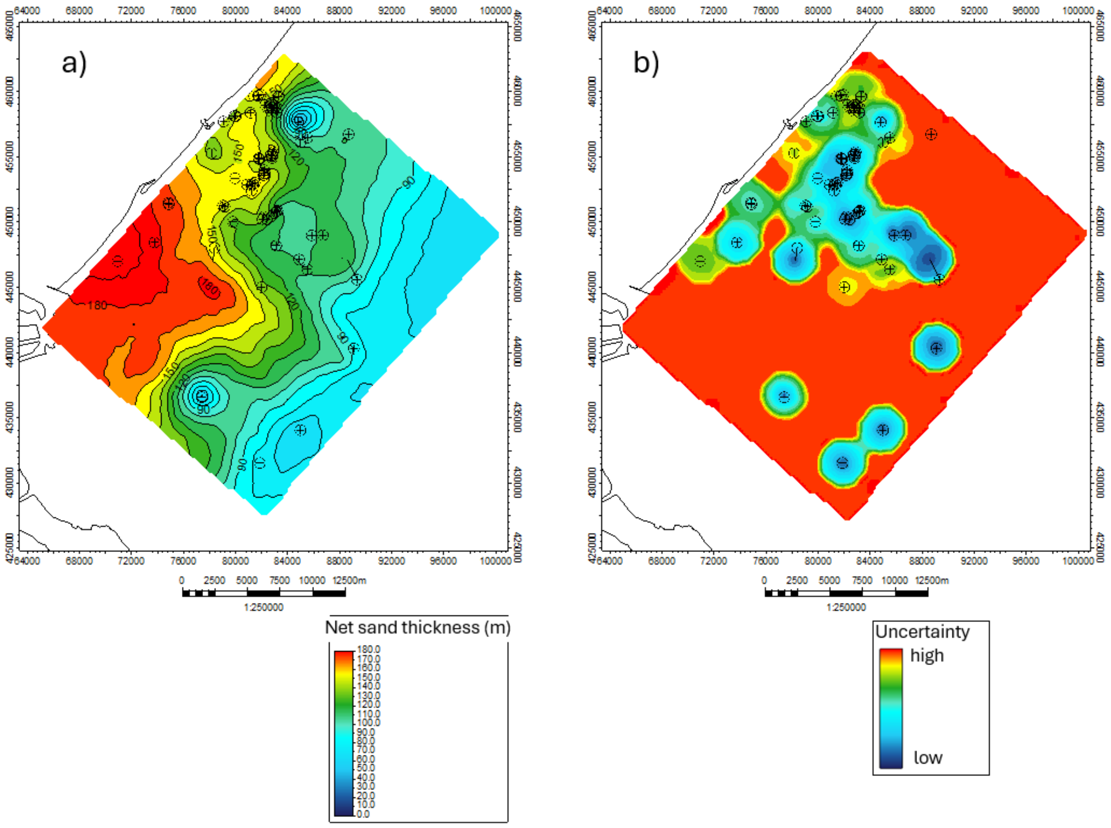


Figure C.5 Sand thickness (a) and qualitative uncertainty in the sand thickness (b) of the upper zone of the SFM surfaces grid with the lithology simulated using SIS with manually set lithology fractions.

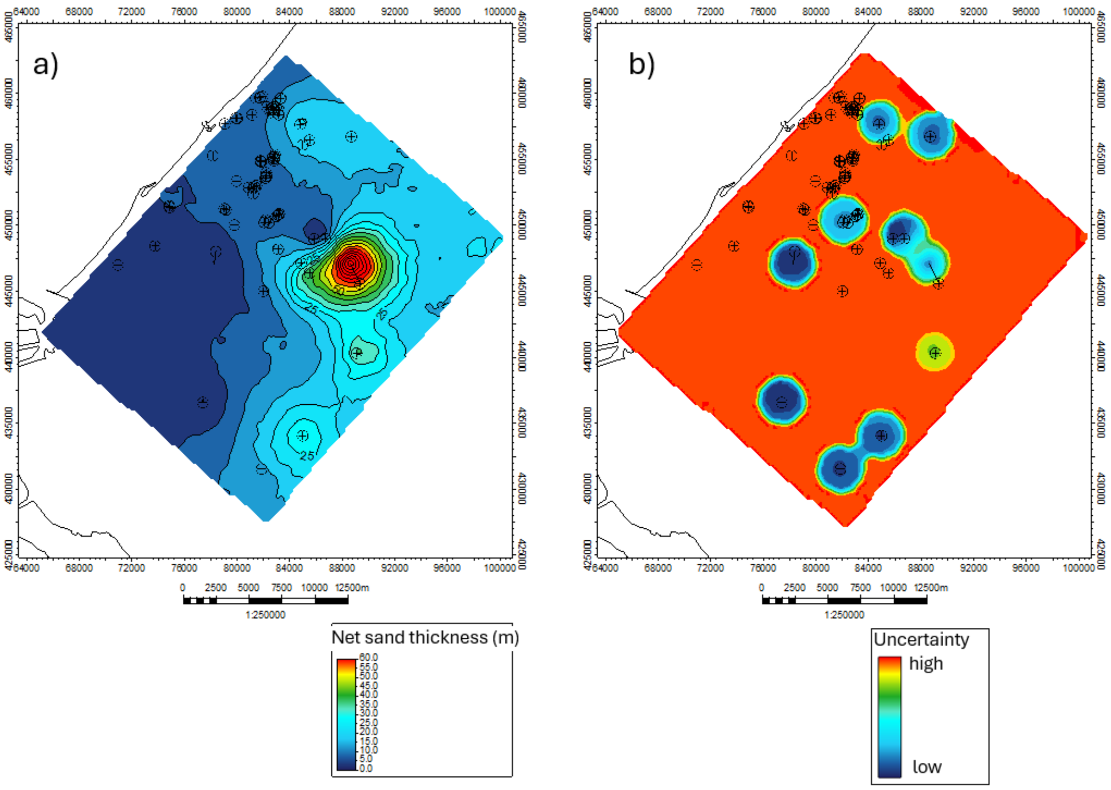


Figure C.6 Sand thickness (a) and qualitative uncertainty in the sand thickness (b) of the upper zone of the SFM surfaces grid with the lithology simulated using SIS with manually set lithology fractions

**Adres**
Princetonlaan 6
3584 CB Utrecht

**Postadres**
Postbus 80015
3508 TA Utrecht

**Telefoon**
088 866 42 56

**E-mail**
contact@warmingup.info

**Website**
www.warmingup.info